Physica A 700 (2026) 131929

Contents lists available at ScienceDirect

Physica A

journal homepage: www.elsevier.com/locate/physa

Banking loan duopoly dynamics with a macroprudential instrument: Bifurcations and virtual fixed points

Moch. Fandi Ansori [a], Serena Brianzoni [b], Giovanni Campisi [b,*]

[a] Department of Mathematics, Faculty of Science and Mathematics, Universitas Diponegoro, Jl. Prof. Jacub Rais, Semarang, 50275, Indonesia
[b] Department of Management, Polytechnic University of Marche, Piazzale R. Martelli 8, Ancona, 60121, Italy

ARTICLE INFO

Keywords:
Stability
Complex dynamics
Loan-to-deposit ratio
Reserve requirement

ABSTRACT

We study the dynamics of a banking loan duopoly under a macroprudential policy based on the loan-to-deposit-ratio reserve requirement (LDR-RR). Unlike previous duopoly contributions focusing on banks with a capital adequacy ratio above the incentive threshold, we consider the case in which the capital ratio remains below that threshold, so that the regulatory mechanism becomes two-sided and reserve requirement penalties may arise both when the loan-to-deposit ratio falls below the lower bound and when it exceeds the upper bound. Starting from a simplified balance-sheet framework, we derive a two-dimensional piecewise-smooth map describing the evolution of the two banks' loan volumes and partition the phase space into nine regions. For each subsystem, we determine the fixed points, distinguish between real and virtual equilibria, and derive existence and local stability conditions. The analysis shows that only three diagonal equilibria may become locally asymptotically stable, while the others are either unstable or always virtual. Instability may arise through both flip (period-doubling) and border-collision bifurcations, depending on the adjustment speed and on the LDR-RR parameters. Numerical simulations support the analytical results and reveal low-period cycles, multistability, and chaotic dynamics. Overall, the results highlight the crucial role played by macroprudential thresholds and penalty coefficients in shaping the stability of aggregate bank lending.

1. Introduction

Bank lending dynamics are inherently nonlinear, since banks continuously revise their loan supply in response to profitability, liquidity conditions, and prudential constraints. When these revisions are modeled through adaptive or gradient-based rules, even simple balance-sheet structures may generate endogenous fluctuations, stability loss, and complex dynamics. For this reason, dynamical models have become a useful framework for studying the interaction between bank behavior and regulation, both in continuous time and in discrete time [1–6].

Within this literature, the Indonesian loan-to-deposit-ratio reserve requirement (LDR-RR) provides an especially interesting case. The policy was first introduced and its microeconomic foundations were analyzed in a seminal paper [7]. This policy links reserve holdings to the bank's intermediation activity and is designed to act as a countercyclical macroprudential instrument: when the LDR is too low, the mechanism encourages lending, whereas when the LDR is too high and capitalization is insufficient, it discourages excessive credit expansion. High or low LDR generally causes banks to exhibit risk-taking behavior in extending credit [8]. The economic rationale of this instrument and its role within the Indonesian macroprudential framework have been discussed from both theoretical and policy-oriented perspectives [1,9–14]. From a dynamical viewpoint, the presence of regulatory thresholds naturally

* Corresponding author.
E-mail address: g.campisi@univpm.it (G. Campisi).

https://doi.org/10.1016/j.physa.2026.131929
Received 9 May 2026; Received in revised form 4 August 2026
Available online 12 August 2026
0378-4371/© 2026 The Authors. Published by Elsevier B.V. This is an open access article under the CC BY license (http://creativecommons.org/licenses/by/4.0/).

Table 1
A simple structure of the Indonesian bank balance sheet.

Financing	Funding
Reserve requirements (R)	Deposits (D)
Loans (L)	
Liquid assets (A)	Equity (E)

leads to piecewise systems, for which border-collision bifurcations and virtual fixed points may play a crucial role in the transition from regular to complex behavior [15,16].

The effects of the LDR-RR on lending dynamics have already been investigated in the monopoly setting by Ansori et al. [9] and, more recently, in a banking duopoly framework by Ansori et al. [15]. However, these contributions focus on the case in which the capital adequacy ratio (CAR) is above the incentive threshold, so that the reserve-requirement penalty is active only when the LDR falls below the lower target bound. Although this assumption is appropriate for well-capitalized banks, it does not fully describe the situation of smaller institutions whose CAR may remain below the incentive threshold while still satisfying the regulatory minimum. In that case, the LDR-RR becomes a two-sided mechanism, because penalties may arise both below the lower bound and above the upper bound. The mechanism of this policy can be tightened or loosened as required [17]. Even banks are allowed to have LDR above the upper target bound if they have a higher CAR and low non-performing loans [18]. This policy is in line with one of the main objectives of macroprudential policies in Indonesia, that is, promoting a well-balanced and sound bank intermediation function [19,20].

In this paper, we extend the duopoly model of [15] to the case of banks with CAR below the incentive threshold. Starting from a simplified balance-sheet representation tailored to the Indonesian setting, we derive a two-dimensional piecewise map for the loan volumes of the two banks and partition the phase space into nine regions. For each subsystem, we determine the fixed points, distinguish between real and virtual equilibria, and derive existence and local stability conditions. The original contributions of the paper are threefold. First, we extend the banking duopoly framework with LDR-RR regulation to the case of banks with CAR below the incentive threshold, thereby obtaining a two-sided macroprudential mechanism. Second, we provide a complete analytical characterization of the resulting piecewise-smooth system in terms of real and virtual fixed points, existence conditions, and local stability properties. Third, we show numerically how the regulatory parameters shape the global dynamics through flip and border-collision bifurcations, multistability, and chaotic regimes.

The analytical results are complemented by numerical simulations. These confirm the theoretical thresholds, illustrate the main bifurcation scenarios associated with the LDR-RR parameters, and show that high adjustment speeds may generate multistability, fragmented basins of attraction, and chaotic lending dynamics. Therefore, the paper provides both a theoretical extension of [15] and a policy-oriented message: when banks operate below the incentive CAR threshold, the calibration of the macroprudential corridor and of the penalty coefficients becomes crucial for the stability of aggregate bank lending.

2. Model of Indonesian banks

The loan-to-deposit ratio reserve requirement (LDR-RR) is a macroprudential instrument implemented in Indonesia. We therefore build our framework on a simplified representation of the balance sheet of an Indonesian bank, whose funding and financing sides are reported in Table 1. Deposits are assumed to include savings deposits, demand deposits, and time deposits. Equity consists of capital, retained earnings, and loss reserves. Reserve requirements (RR) include primary RR, secondary RR, and LDR-RR. The first component is mainly related to monetary policy, the second to liquidity policy, and the third to macroprudential policy. Loans are the asset component generating the highest income, but they are also associated with the procyclical behavior of banks. Since the LDR-RR acts as a countercyclical macroprudential instrument, our main goal is to investigate its role in the dynamics of bank lending. Finally, liquid assets are treated as the balancing item of the balance sheet.

The funding and financing sides must balance, that is, $R + L + A = D + E$. Since liquid assets are assumed to be the balancing variable, it follows that

$$A = D + E - (R + L).$$

The main variable studied in this paper is the volume of loans. Loan dynamics can be modeled either in continuous time [1,2] or in discrete time [3–5]. Here we adopt the latter approach, since it is particularly suitable for capturing the procyclical behavior of bank lending, whereas the LDR-RR is explicitly designed as a countercyclical policy tool. The discrete-time model is given by:

$$L_{t+1} = L_t + \alpha L_t \frac{\partial \pi_t}{\partial L_t}, \tag{1}$$

where π_t denotes bank profit and $\alpha > 0$ is the speed of adjustment parameter. When economic conditions are favorable, which can be represented by $\partial \pi_t / \partial L_t > 0$, the bank expands lending. Conversely, when conditions deteriorate and $\partial \pi_t / \partial L_t < 0$, the bank contracts lending. If α is excessively large, the bank reacts too aggressively, expanding lending too much during upswings and reducing it too sharply during downturns. For this reason, α can be interpreted as an index of the bank's procyclicality.

We assume that bank profit is given by:

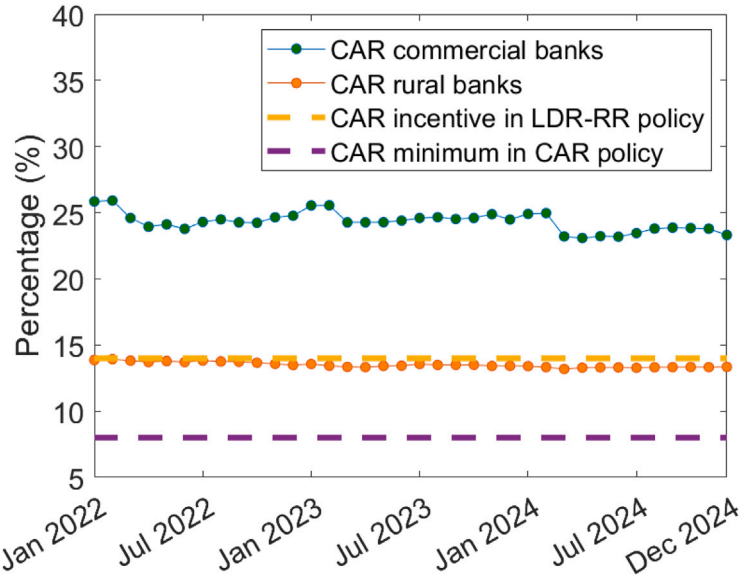


Fig. 1. CAR data for Indonesian commercial and rural banks from January 2022 - December 2024.

$$\pi = r_L L + r_A A - r_D D - r_E E - C, \tag{2}$$

where $r_L = a - bL$ with $a, b > 0$ is the loan interest rate, $0 < r_A < 1$ is the rate of return on liquid assets, r_D is the deposit interest rate, $0 < r_E < 1$ is an equity cost, and $C = c(D + L)$ with $0 < c < 1$ denotes operational costs.

Reserve requirements are a regulatory policy requiring banks to hold a certain fraction of deposits at the central bank. This minimum fraction is set by the monetary authority. In Indonesia, banks may receive interest on reserves exceeding the required minimum. In this paper, however, we restrict attention to the case in which reserve holdings are exactly equal to the required minimum, so that no interest is paid on RR. Consequently, RR does not directly enter the profit function. Let $0 < \rho_p < 1$ and $0 < \rho_s < 1$ denote the minimum required ratios for primary RR (R^P) and secondary RR (R^S), respectively. Then,

$$R^P = \rho_p D, \qquad R^S = \rho_s D.$$

Hence, total reserve requirements in Indonesia can be written as

$$R = (\rho_p + \rho_s)D + R^{LDR},$$

where R^{LDR} denotes the LDR-RR component. According to the Bank Indonesia regulation on LDR-RR [21], the latter is computed as

$$R^{LDR} = \begin{cases} 0, & \text{if } \delta_{lb} \le L/D \le \delta_{ub} \\ \gamma_{lb}\left(\delta_{lb} - \frac{L}{D}\right) D, & \text{if } L/D < \delta_{lb} \\ \gamma_{ub}\left(\frac{L}{D} - \delta_{ub}\right) D, & \text{if } L/D > \delta_{ub} \text{ and } E/L < \kappa_{ldr} \\ 0, & \text{if } L/D > \delta_{ub} \text{ and } E/L \ge \kappa_{ldr}, \end{cases} \tag{3}$$

where δ_{lb}, δ_{ub}, κ_{ldr}, γ_{lb}, and γ_{ub} are policy parameters representing, respectively, the lower target bound for the bank's LDR, the upper target bound, the incentive capital adequacy ratio (CAR). The penalty applied when the LDR is below the target range, and the penalty applied when the LDR exceeds the upper bound while the CAR remains below the incentive threshold. These parameters satisfy

$$0 < \delta_{lb} < \delta_{ub}, \qquad 0 < \kappa_{ldr} < 1, \qquad \gamma_{lb}, \gamma_{ub} > 0.$$

The CAR data for Indonesian commercial and rural banks are shown in Fig. 1. The data are obtained from [22]. On average, commercial banks exhibit a CAR above the regulated incentive threshold (14%), whereas rural banks exhibit a CAR below that level. Motivated by this evidence, we may regard larger banks (commercial banks) as institutions with CAR above the incentive threshold, while smaller banks (rural banks) can be viewed as institutions with CAR below it. If a bank has a CAR above the incentive threshold, then (3) reduces to

$$R^{LDR} = \begin{cases} 0, & \text{if } L/D \ge \delta_{lb} \\ \gamma_{lb}\left(\delta_{lb} - \frac{L}{D}\right) D, & \text{if } L/D < \delta_{lb}. \end{cases} \tag{4}$$

The dynamics of bank lending in the case of a bank with CAR above the incentive threshold, leading to the LDR-RR specification in (4), have already been investigated by Ansori et al. [9] in the monopoly setting and by Ansori et al. [15] in the duopoly setting.

In this paper, we focus instead on the case in which the bank's CAR is below the incentive threshold. In that case, (3) becomes

$$R^{LDR} = \begin{cases} \gamma_{lb}\left(\delta_{lb} - \frac{L}{D}\right) D, & \text{if } L/D < \delta_{lb} \\ \gamma_{ub}\left(\frac{L}{D} - \delta_{ub}\right) D, & \text{if } L/D > \delta_{ub} \\ 0, & \text{if } \delta_{lb} \le L/D \le \delta_{ub}. \end{cases} \tag{5}$$

Our aim is to investigate the role played by the LDR-RR parameters δ_{lb}, δ_{ub}, γ_{lb}, and γ_{ub} in shaping the dynamics of bank lending.

Equity is also constrained by the CAR regulation, according to which

$$E/L \ge \kappa_{car},$$

where $0 < \kappa_{car} < 1$ is the minimum CAR imposed by the regulator. As shown in Fig. 1, although rural banks exhibit an average CAR below the incentive threshold (14%), they still remain above the regulatory minimum CAR (8%) [23]. To simplify the analysis and keep the model tractable, we assume that

$$E/L = \kappa, \quad \kappa_{car} \le \kappa < \kappa_{ldr},$$

where κ is constant.

Following [9], deposits are assumed to evolve according to a discrete logistic law:

$$D_{t+1} = D_t + \beta D_t\left(1 - \frac{D_t}{K}\right), \qquad \beta, K > 0. \tag{6}$$

Under the above assumptions, the bank's profit at time t is

$$\begin{aligned} \pi_t &= (a - bL_t)L_t + r_A(D_t + E_t - R_t - L_t) - r_D D_t - r_E E_t - (cD_t + cL_t) \\ &= \begin{cases} (a - \Lambda + r_A\gamma_{lb})L_t - bL_t^2 + [r_A - r_D - c - r_A(\rho_p + \rho_s + \gamma_{lb}\delta_{lb})]D_t, & \text{if } L_t/D_t < \delta_{lb} \\ (a - \Lambda - r_A\gamma_{ub})L_t - bL_t^2 + [r_A - r_D - c - r_A(\rho_p + \rho_s - \gamma_{ub}\delta_{ub})]D_t, & \text{if } L_t/D_t > \delta_{ub} \\ (a - \Lambda)L_t - bL_t^2 + [r_A - r_D - c - r_A(\rho_p + \rho_s)]D_t, & \text{if } \delta_{lb} \le L_t/D_t \le \delta_{ub}, \end{cases} \end{aligned}$$

where $\Lambda = r_A(1 - \kappa) + r_E\kappa + c$.

Therefore, the marginal profit with respect to loans is

$$\frac{\partial \pi_t}{\partial L_t} = \begin{cases} a - \Lambda + r_A\gamma_{lb} - 2bL_t, & \text{if } L_t/D_t < \delta_{lb} \\ a - \Lambda - r_A\gamma_{ub} - 2bL_t, & \text{if } L_t/D_t > \delta_{ub} \\ a - \Lambda - 2bL_t, & \text{if } \delta_{lb} \le L_t/D_t \le \delta_{ub}. \end{cases}$$

Combining the deposit and loan equations yields the following two-dimensional map:

$$T_0 := \begin{cases} D_{t+1} = D_t + \beta D_t\left(1 - \frac{D_t}{K}\right) \\ L_{t+1} = \begin{cases} L_t + \alpha L_t\left(a - \Lambda + r_A\gamma_{lb} - 2bL_t\right), & \text{if } L_t/D_t < \delta_{lb} \\ L_t + \alpha L_t\left(a - \Lambda - r_A\gamma_{ub} - 2bL_t\right), & \text{if } L_t/D_t > \delta_{ub} \\ L_t + \alpha L_t\left(a - \Lambda - 2bL_t\right), & \text{if } \delta_{lb} \le L_t/D_t \le \delta_{ub} \end{cases} \end{cases}.$$

Since the deposit equation in T_0 is independent of the loan variable, the deposit dynamics in Eq. (6) can be analyzed separately. The positive fixed point of Eq. (6) is $D^* = K$, and the derivative of the right-hand side at this point is $1 - \beta$. Hence, K is locally asymptotically stable for $0 < \beta < 2$. Moreover, for $D_t > 0$, the next iterate remains positive provided

$$D_t < K\left(1 + \frac{1}{\beta}\right).$$

Thus, in what follows, we assume $0 < \beta < 2$ and economically meaningful initial deposit levels, for instance $0 < D_0 < K(1 + 1/\beta)$, so that the deposit dynamics remains positive and converges to K. The reduction $D_t = K$ is then based on a time-scale separation assumption. Economically, deposits represent the relatively stable funding base of the bank and are not the strategic variable of the duopoly game, whereas loans are adjusted through profit-driven decisions, competitive interaction, and regulatory thresholds. Therefore, over the time scale on which banks revise their loan supply, the deposit base is treated as having already reached, or being sufficiently close to, its long-run level K. Under this time-scale separation assumption, T_0 reduces to the one-dimensional piecewise map

$$T := \begin{cases} L_{t+1} = L_t + \alpha L_t\left(a - \Lambda + r_A\gamma_{lb} - 2bL_t\right), & \text{if } L_t < \delta_{lb}K \\ L_{t+1} = L_t + \alpha L_t\left(a - \Lambda - r_A\gamma_{ub} - 2bL_t\right), & \text{if } L_t > \delta_{ub}K \\ L_{t+1} = L_t + \alpha L_t\left(a - \Lambda - 2bL_t\right), & \text{if } \delta_{lb}K \le L_t \le \delta_{ub}K. \end{cases} \tag{7}$$

Following the banking duopoly framework introduced in [15], we now extend (7) to the duopoly case. Let there be two banks indexed by $k = 1, 2$. We consider a homogeneous rational-expectations banking duopoly [3] described by

$$S := \begin{cases} L_{1,t+1} = L_{1,t} + \alpha L_{1,t} \dfrac{\partial \pi_{1,t}(L_{1,t}, L_{2,t})}{\partial L_{1,t}} \\ L_{2,t+1} = L_{2,t} + \alpha L_{2,t} \dfrac{\partial \pi_{2,t}(L_{1,t}, L_{2,t})}{\partial L_{2,t}}, \end{cases} \tag{8}$$

where the loan interest rate is now assumed to depend on total loan supply according to

$$r_{L,t} = a - b(L_{1,t} + L_{2,t}).$$

Accordingly, the map in (8) becomes

$$S := \begin{cases} L_{1,t+1} = \begin{cases} L_{1,t} + \alpha L_{1,t} \left(a - \Lambda + r_A \gamma_{lb} - bL_{2,t} - 2bL_{1,t}\right), & \text{if } L_{1,t} < \delta_{lb} K \\ L_{1,t} + \alpha L_{1,t} \left(a - \Lambda - r_A \gamma_{ub} - bL_{2,t} - 2bL_{1,t}\right), & \text{if } L_{1,t} > \delta_{ub} K \\ L_{1,t} + \alpha L_{1,t} \left(a - \Lambda - bL_{2,t} - 2bL_{1,t}\right), & \text{if } \delta_{lb} K \le L_{1,t} \le \delta_{ub} K \end{cases} \\ L_{2,t+1} = \begin{cases} L_{2,t} + \alpha L_{2,t} \left(a - \Lambda + r_A \gamma_{lb} - bL_{1,t} - 2bL_{2,t}\right), & \text{if } L_{2,t} < \delta_{lb} K \\ L_{2,t} + \alpha L_{2,t} \left(a - \Lambda - r_A \gamma_{ub} - bL_{1,t} - 2bL_{2,t}\right), & \text{if } L_{2,t} > \delta_{ub} K \\ L_{2,t} + \alpha L_{2,t} \left(a - \Lambda - bL_{1,t} - 2bL_{2,t}\right), & \text{if } \delta_{lb} K \le L_{2,t} \le \delta_{ub} K. \end{cases} \end{cases} \tag{9}$$

We divide the phase space of map S in (9) into nine regions:

$$\begin{aligned} \Omega_1 &= \{(L_1, L_2) \in \mathbb{R}^2_+ : L_1 < \delta_{lb} K, L_2 < \delta_{lb} K\}, \\ \Omega_2 &= \{(L_1, L_2) \in \mathbb{R}^2_+ : L_1 < \delta_{lb} K, L_2 > \delta_{ub} K\}, \\ \Omega_3 &= \{(L_1, L_2) \in \mathbb{R}^2_+ : L_1 < \delta_{lb} K, \delta_{lb} K \le L_2 \le \delta_{ub} K\}, \\ \Omega_4 &= \{(L_1, L_2) \in \mathbb{R}^2_+ : L_1 > \delta_{ub} K, L_2 < \delta_{lb} K\}, \\ \Omega_5 &= \{(L_1, L_2) \in \mathbb{R}^2_+ : L_1 > \delta_{ub} K, L_2 > \delta_{ub} K\}, \\ \Omega_6 &= \{(L_1, L_2) \in \mathbb{R}^2_+ : L_1 > \delta_{ub} K, \delta_{lb} K \le L_2 \le \delta_{ub} K\}, \\ \Omega_7 &= \{(L_1, L_2) \in \mathbb{R}^2_+ : \delta_{lb} K \le L_1 \le \delta_{ub} K, L_2 < \delta_{lb} K\}, \\ \Omega_8 &= \{(L_1, L_2) \in \mathbb{R}^2_+ : \delta_{lb} K \le L_1 \le \delta_{ub} K, L_2 > \delta_{ub} K\}, \\ \Omega_9 &= \{(L_1, L_2) \in \mathbb{R}^2_+ : \delta_{lb} K \le L_1 \le \delta_{ub} K, \delta_{lb} K \le L_2 \le \delta_{ub} K\}. \end{aligned}$$

These regions are separated by the set $\Omega = \{(L_1, L_2) \in \mathbb{R}^2_+ : L_1 = \delta_{lb} K\} \cup \{(L_1, L_2) \in \mathbb{R}^2_+ : L_1 = \delta_{ub} K\} \cup \{(L_1, L_2) \in \mathbb{R}^2_+ : L_2 = \delta_{lb} K\} \cup \{(L_1, L_2) \in \mathbb{R}^2_+ : L_2 = \delta_{ub} K\}$.

Hence, the region boundaries are represented by the horizontal lines $L_2 = \delta_{lb} K$ and $L_2 = \delta_{ub} K$, and by the vertical lines $L_1 = \delta_{lb} K$ and $L_1 = \delta_{ub} K$; see Fig. 2.

This partition has a direct economic interpretation. For each bank, the lower region $L_k < \delta_{lb} K$ corresponds to an under-lending position, in which the bank's LDR is below the lower target and the lower-side LDR-RR penalty is active. The upper region $L_k > \delta_{ub} K$ corresponds to an over-lending position, in which the bank exceeds the upper LDR bound and, since its CAR is below the incentive threshold, faces the upper-side penalty. The middle region $\delta_{lb} K \le L_k \le \delta_{ub} K$ represents the regulatory target corridor, where no LDR-RR penalty is applied.

Accordingly, each region Ω_i describes a specific competitive and regulatory configuration of the two banks. For instance, in Ω_2 bank 1 under-lends whereas bank 2 over-lends. The two banks are therefore subject to opposite regulatory incentives: the first is encouraged to expand lending, while the second is discouraged from further credit expansion. Regions Ω_1, Ω_5, and Ω_9 describe symmetric configurations in which both banks are respectively below the lower bound, above the upper bound, or inside the target corridor. The remaining regions capture asymmetric market situations, where only one bank is outside the corridor or the two banks violate opposite bounds. From a policy perspective, these asymmetric regions are especially relevant because the LDR-RR mechanism may affect not only aggregate lending but also the competitive balance between banks by imposing different marginal incentives on institutions located in different parts of the regulatory corridor.

Because of this partition, map S can be represented by the following nine subsystems:

1. System 1, for all $(L_1, L_2) \in \Omega_1$

$$S_1 := \begin{cases} L_{1,t+1} = L_{1,t} + \alpha L_{1,t} \left(a - \Lambda + r_A \gamma_{lb} - bL_{2,t} - 2bL_{1,t}\right) \\ L_{2,t+1} = L_{2,t} + \alpha L_{2,t} \left(a - \Lambda + r_A \gamma_{lb} - bL_{1,t} - 2bL_{2,t}\right) \end{cases} \tag{10}$$

2. System 2, for all $(L_1, L_2) \in \Omega_2$

$$S_2 := \begin{cases} L_{1,t+1} = L_{1,t} + \alpha L_{1,t} \left(a - \Lambda + r_A \gamma_{lb} - bL_{2,t} - 2bL_{1,t}\right) \\ L_{2,t+1} = L_{2,t} + \alpha L_{2,t} \left(a - \Lambda - r_A \gamma_{ub} - bL_{1,t} - 2bL_{2,t}\right) \end{cases} \tag{11}$$

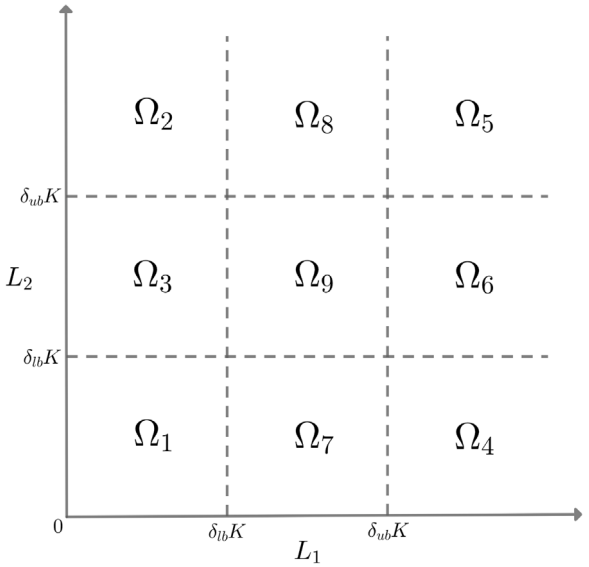


Fig. 2. Phase-space partition into the nine economic-regulatory configurations associated with System i, $i = 1, 2, \ldots, 9$.

3. System 3, for all $(L_1, L_2) \in \Omega_3$

$$S_3 := \begin{cases} L_{1,t+1} = L_{1,t} + \alpha L_{1,t}\left(a - \Lambda + r_A\gamma_{lb} - bL_{2,t} - 2bL_{1,t}\right) \\ L_{2,t+1} = L_{2,t} + \alpha L_{2,t}\left(a - \Lambda - bL_{1,t} - 2bL_{2,t}\right) \end{cases} \tag{12}$$

4. System 4, for all $(L_1, L_2) \in \Omega_4$

$$S_4 := \begin{cases} L_{1,t+1} = L_{1,t} + \alpha L_{1,t}\left(a - \Lambda - r_A\gamma_{ub} - bL_{2,t} - 2bL_{1,t}\right) \\ L_{2,t+1} = L_{2,t} + \alpha L_{2,t}\left(a - \Lambda + r_A\gamma_{lb} - bL_{1,t} - 2bL_{2,t}\right) \end{cases} \tag{13}$$

5. System 5, for all $(L_1, L_2) \in \Omega_5$

$$S_5 := \begin{cases} L_{1,t+1} = L_{1,t} + \alpha L_{1,t}\left(a - \Lambda - r_A\gamma_{ub} - bL_{2,t} - 2bL_{1,t}\right) \\ L_{2,t+1} = L_{2,t} + \alpha L_{2,t}\left(a - \Lambda - r_A\gamma_{ub} - bL_{1,t} - 2bL_{2,t}\right) \end{cases} \tag{14}$$

6. System 6, for all $(L_1, L_2) \in \Omega_6$

$$S_6 := \begin{cases} L_{1,t+1} = L_{1,t} + \alpha L_{1,t}\left(a - \Lambda - r_A\gamma_{ub} - bL_{2,t} - 2bL_{1,t}\right) \\ L_{2,t+1} = L_{2,t} + \alpha L_{2,t}\left(a - \Lambda - bL_{1,t} - 2bL_{2,t}\right) \end{cases} \tag{15}$$

7. System 7, for all $(L_1, L_2) \in \Omega_7$

$$S_7 := \begin{cases} L_{1,t+1} = L_{1,t} + \alpha L_{1,t}\left(a - \Lambda - bL_{2,t} - 2bL_{1,t}\right) \\ L_{2,t+1} = L_{2,t} + \alpha L_{2,t}\left(a - \Lambda + r_A\gamma_{lb} - bL_{1,t} - 2bL_{2,t}\right) \end{cases} \tag{16}$$

8. System 8, for all $(L_1, L_2) \in \Omega_8$

$$S_8 := \begin{cases} L_{1,t+1} = L_{1,t} + \alpha L_{1,t}\left(a - \Lambda - bL_{2,t} - 2bL_{1,t}\right) \\ L_{2,t+1} = L_{2,t} + \alpha L_{2,t}\left(a - \Lambda - r_A\gamma_{ub} - bL_{1,t} - 2bL_{2,t}\right) \end{cases} \tag{17}$$

9. System 9, for all $(L_1, L_2) \in \Omega_9$

$$S_9 := \begin{cases} L_{1,t+1} = L_{1,t} + \alpha L_{1,t}\left(a - \Lambda - bL_{2,t} - 2bL_{1,t}\right) \\ L_{2,t+1} = L_{2,t} + \alpha L_{2,t}\left(a - \Lambda - bL_{1,t} - 2bL_{2,t}\right). \end{cases} \tag{18}$$

We note that System 4 is the reflection of System 2 with respect to the line $L_1 = L_2$, System 7 is the reflection of System 3 with respect to the same line, and System 8 is the reflection of System 6. Therefore, the analysis of System 4 is analogous to that of System 2, the analysis of System 7 is analogous to that of System 3, and the analysis of System 8 is analogous to that of System 6.

For each bank, the update rule can be written as

$$L_{k,t+1} = L_{k,t}\left[1 + \alpha\left(\xi_k - bL_{j,t} - 2bL_{k,t}\right)\right], \qquad k, j = 1, 2,\ k \neq j,$$

where

$$\xi_k \in \left\{a - \Lambda + r_A\gamma_{lb},\ a - \Lambda,\ a - \Lambda - r_A\gamma_{ub}\right\}.$$

Hence, if $L_{k,t} \geq 0$, then $L_{k,t+1} \geq 0$ whenever

$$1 + \alpha\left(\xi_k - bL_{j,t} - 2bL_{k,t}\right) \geq 0.$$

Equivalently,

$$2bL_{k,t} + bL_{j,t} \leq \xi_k + \frac{1}{\alpha}.$$

Thus, for a given active subsystem, membership in the corresponding set

$$P_\alpha = \left\{(L_1, L_2) \in \mathbb{R}^2_+ : 2bL_1 + bL_2 \leq \xi_1 + \frac{1}{\alpha},\ bL_1 + 2bL_2 \leq \xi_2 + \frac{1}{\alpha}\right\}$$

provides a sufficient one-step condition for the next iterate to remain nonnegative, with the appropriate values of ξ_1 and ξ_2 determined by the active subsystem. However, this condition should not be interpreted as the construction of a positively invariant bounded region, since an iterate satisfying the condition at time t may leave the corresponding set at time $t + 1$. Therefore, in the numerical simulations below, positivity and boundedness are verified explicitly along the computed trajectories. In particular, trajectories that leave $\mathbb{R}^2_+$, become nonfinite, or exceed the prescribed divergence threshold are not classified as economically meaningful asymptotic dynamics.

3. Fixed points, stability, and bifurcations

A fixed point is called a *real fixed point* if it belongs to the region associated with the corresponding subsystem, whereas it is called a *virtual fixed point* if it is generated by that subsystem but lies outside its defining region [24]. The fixed points of the proposed systems S_i, $i = 1, 2, \ldots, 9$, are obtained by solving

$$L_{k,t+1} - L_{k,t} = 0, \qquad k = 1, 2,$$

for all t. Observe that all systems admit the trivial fixed point $(0, 0)$; however, it is real only for System 1 and virtual for the remaining systems. Let $\mathbb{E}_{ij} = (L_1^*, L_2^*)$ denote the jth nontrivial fixed point of System i, and let $\mathbb{E}_{10} = (0, 0)$ denote the trivial one. In the following analysis, we distinguish between positive interior equilibria, for which $L_1^* > 0$ and $L_2^* > 0$, and nonnegative boundary equilibria, for which at least one bank has zero loans while the other loan volume is nonnegative. The former describe configurations in which both banks are active in the loan market, whereas the latter are economically meaningful only as boundary cases and are included for mathematical completeness. Thus, the term "positive equilibrium" will be used only for interior equilibria, while boundary equilibria will be explicitly identified as nonnegative boundary fixed points.

Next, we denote by J the Jacobian matrix of each system, where J is a 2×2 matrix. The Jacobian matrix evaluated at the fixed point $\mathbb{E}_{ij}$ is denoted by J_{ij}. Let λ_1 and λ_2 denote the eigenvalues of J.

A fixed point is locally asymptotically stable if $|\lambda_k| < 1$, $k = 1, 2$, and it is unstable if at least one eigenvalue has modulus greater than one. In particular, the fixed point is a saddle point if $|\lambda_1| < 1$ and $|\lambda_2| > 1$, regardless of the order of the eigenvalues.

For those fixed points that may be stable, and in order to connect the analysis with bifurcation theory, we study their stability using the following Jury stability conditions [25]:

$$\begin{cases} F := 1 + \mathrm{tr}(J) + \det(J) > 0 \\ T := 1 - \mathrm{tr}(J) + \det(J) > 0 \\ N := 1 - \det(J) > 0, \end{cases} \tag{19}$$

where $\mathrm{tr}(J)$ and $\det(J)$ denote the trace and the determinant of J, respectively. The conditions $F = 0$, $T = 0$, and $N = 0$ correspond to the presence of an eigenvalue -1, an eigenvalue $+1$, and eigenvalues on the unit circle, respectively. Whether these conditions lead to a particular bifurcation depends on additional nonresonance and transversality conditions.

Moreover, since our systems are characterized by borders, we also consider the so-called border-collision bifurcation, which occurs when a fixed point collides with the border. The stability analysis will be carried out by deriving conditions (when they exist) with respect to the LDR-RR parameters in (5): γ_{lb}, γ_{ub}, δ_{lb}, and δ_{ub}.

3.1. System 1

The fixed points are

$$\mathbb{E}_{11} = \left(0, \frac{a - \Lambda + r_A\gamma_{lb}}{2b}\right), \quad \mathbb{E}_{12} = \left(\frac{a - \Lambda + r_A\gamma_{lb}}{2b}, 0\right), \quad \text{and}$$
$$\mathbb{E}_{13} = \left(\frac{a - \Lambda + r_A\gamma_{lb}}{3b}, \frac{a - \Lambda + r_A\gamma_{lb}}{3b}\right).$$

The boundary equilibria have nonnegative coordinates, and the interior equilibrium has strictly positive coordinates, if

$$a > \Lambda - r_A\gamma_{lb}. \tag{20}$$

Recall the definition of the region Ω_1. Note that $\mathbb{E}_{11}$ and $\mathbb{E}_{12}$ are real fixed points if $\frac{a-\Lambda+r_A\gamma_{lb}}{2b} < \delta_{lb}K$, and virtual otherwise. Meanwhile, $\mathbb{E}_{13}$ is a real fixed point if $\frac{a-\Lambda+r_A\gamma_{lb}}{3b} < \delta_{lb}K$, and virtual otherwise. Hence, parameter b plays a crucial role in determining whether $\mathbb{E}_{1j}$, $j = 1, 2, 3$, is a real or a virtual fixed point.

The Jacobian matrix evaluated at the real fixed point (L_1^*, L_2^*) is

$$J = \begin{bmatrix} 1 + \alpha(a - \Lambda + r_A\gamma_{lb}) - \alpha b L_2^* - 4\alpha b L_1^* & -\alpha b L_1^* \\ -\alpha b L_2^* & 1 + \alpha(a - \Lambda + r_A\gamma_{lb}) - \alpha b L_1^* - 4\alpha b L_2^* \end{bmatrix}.$$

In the case of real fixed points, we have the following result.

Theorem 1. *The trivial fixed point $\mathbb{E}_{10} = (0, 0)$ is unstable, and:*

1. *If $\frac{a-\Lambda+r_A\gamma_{lb}}{2b} < \delta_{lb}K$, then $\mathbb{E}_{11} = \left(0, \frac{a-\Lambda+r_A\gamma_{lb}}{2b}\right)$ and $\mathbb{E}_{12} = \left(\frac{a-\Lambda+r_A\gamma_{lb}}{2b}, 0\right)$ are unstable.*
2. *If $\frac{a-\Lambda+r_A\gamma_{lb}}{3b} < \delta_{lb}K$, then $\mathbb{E}_{13} = \left(\frac{a-\Lambda+r_A\gamma_{lb}}{3b}, \frac{a-\Lambda+r_A\gamma_{lb}}{3b}\right)$ is locally asymptotically stable for $\gamma_{lb} < \frac{1}{\alpha r_A}[2 - \alpha(a - \Lambda)]$.*

Proof. Let

$$\theta_1 = \alpha(a - \Lambda + r_A\gamma_{lb}). \tag{21}$$

From (20), it follows that $\theta_1 > 0$. In the case of $\mathbb{E}_{10}$, the Jacobian matrix is

$$J_{10} = \begin{bmatrix} 1 + \theta_1 & 0 \\ 0 & 1 + \theta_1 \end{bmatrix}.$$

The eigenvalues are $\lambda_1 = \lambda_2 = 1 + \theta_1 > 1$. Thus, $\mathbb{E}_{10}$ is unstable.

The Jacobian matrix evaluated at $\mathbb{E}_{11}$ is

$$J_{11} = \begin{bmatrix} 1 + \frac{1}{2}\theta_1 & 0 \\ -\frac{1}{2}\theta_1 & 1 - \theta_1 \end{bmatrix}.$$

The eigenvalues are $\lambda_1 = 1 + \frac{1}{2}\theta_1 > 1$ and $\lambda_2 = 1 - \theta_1$, so $\mathbb{E}_{11}$ is unstable. In particular, it is a saddle point when $\theta_1 < 2$.

The case of $\mathbb{E}_{12}$ is analogous to that of $\mathbb{E}_{11}$. Hence, $\mathbb{E}_{12}$ is also unstable and a saddle point when $\theta_1 < 2$.

Finally, in case of $\mathbb{E}_{13}$, the Jacobian matrix is

$$J_{13} = \begin{bmatrix} 1 - \frac{2}{3}\theta_1 & -\frac{1}{3}\theta_1 \\ -\frac{1}{3}\theta_1 & 1 - \frac{2}{3}\theta_1 \end{bmatrix}.$$

We have $\mathrm{tr}(J_{13}) = 2 - \frac{4}{3}\theta_1$ and $\det(J_{13}) = 1 - \frac{4}{3}\theta_1 + \frac{1}{3}\theta_1^2$. The Jury stability conditions are

$$F = 4 - \frac{8}{3}\theta_1 + \frac{1}{3}\theta_1^2 = \frac{1}{3}[(\theta_1 - 4)^2 - 4] > 0 \quad \text{if} \quad \theta_1 < 2 \text{ or } \theta_1 > 6,$$
$$T = \frac{1}{3}\theta_1^2 > 0,$$
$$N = \frac{4}{3}\theta_1 - \frac{1}{3}\theta_1^2 > 0 \quad \text{if} \quad \theta_1 < 4.$$

These conditions hold if $\theta_1 < 2$, which is equivalent to

$$\gamma_{lb} < \frac{1}{\alpha r_A}[2 - \alpha(a - \Lambda)]. \tag{22}$$

Therefore, $\mathbb{E}_{13}$ is locally asymptotically stable if condition (22) holds. □

The stable fixed point $\mathbb{E}_{13}$ may undergo a flip bifurcation when $\gamma_{lb} = \gamma_{lb}^F$, where

$$\gamma_{lb}^F = \frac{1}{\alpha r_A}[2 - \alpha(a - \Lambda)].$$

Hence, $\mathbb{E}_{13}$ is stable if $\gamma_{lb} < \gamma_{lb}^F$.

Next, we study the border-collision bifurcation of $\mathbb{E}_{13} = (L_1^*, L_2^*)$. System 1 has borders $L_1 = \delta_{lb}K$ and $L_2 = \delta_{lb}K$. The fixed point $\mathbb{E}_{13}$ may undergo a border-collision bifurcation when

$$\frac{a - \Lambda + r_A\gamma_{lb}}{3b} = \delta_{lb}K.$$

This condition is equivalent to $\gamma_{lb} = \gamma_{lb}^B$, where

$$\gamma_{lb}^B = \frac{1}{r_A}[3b\delta_{lb}K - (a - \Lambda)],$$

or $\delta_{lb} = \delta_{lb}^{B_1}$, where

$$\delta_{lb}^{B_1} = \frac{a - \Lambda + r_A \gamma_{lb}}{3bK}.$$

In this case, $\mathbb{E}_{13}$ must satisfy $L_1^* < \delta_{lb} K$ and $L_2^* < \delta_{lb} K$, i.e.,

$$\gamma_{lb} < \gamma_{lb}^B \quad \text{or} \quad \delta_{lb} > \delta_{lb}^{B_1}.$$

From this analysis, if $\gamma_{lb}^F < \gamma_{lb}^B$, then $\mathbb{E}_{13}$ loses stability only through a flip bifurcation; otherwise, it loses stability through a border-collision bifurcation. This result is summarized in the following theorem.

Theorem 2. *Suppose $\gamma_{lb}^F > 0$ and $\gamma_{lb}^B > 0$,*

1. *if $\gamma_{lb}^F < \gamma_{lb}^B$, then $\mathbb{E}_{13}$ is stable for $\gamma_{lb} < \gamma_{lb}^F$ and loses stability through a flip bifurcation when $\gamma_{lb} = \gamma_{lb}^F$;*
2. *if $\gamma_{lb}^B < \gamma_{lb}^F$, then $\mathbb{E}_{13}$ is stable for $\gamma_{lb} < \gamma_{lb}^B$ and loses stability through a border-collision bifurcation when $\gamma_{lb} = \gamma_{lb}^B$.*

3.2. System 2 and System 4

The fixed points of System 2 are

$$\mathbb{E}_{21} = \left(0, \frac{a - \Lambda - r_A \gamma_{ub}}{2b}\right), \quad \mathbb{E}_{22} = \left(\frac{a - \Lambda + r_A \gamma_{lb}}{2b}, 0\right), \quad \text{and}$$
$$\mathbb{E}_{23} = \left(\frac{a - \Lambda + 2r_A \gamma_{lb} + r_A \gamma_{ub}}{3b}, \frac{a - \Lambda - r_A \gamma_{lb} - 2r_A \gamma_{ub}}{3b}\right).$$

The boundary equilibria have nonnegative coordinates, and the interior equilibrium has strictly positive coordinates, if

$$a > \Lambda + r_A \gamma_{lb} + 2r_A \gamma_{ub}. \tag{23}$$

Recall the definition of the region Ω_2. The conditions defining Ω_2 imply that

$$L_1 < \delta_{lb} K < \delta_{ub} K < L_2.$$

Hence, $\mathbb{E}_{22}$ and $\mathbb{E}_{23}$ are always virtual fixed points, whereas $\mathbb{E}_{21}$ is a real fixed point if

$$\frac{a - \Lambda - r_A \gamma_{ub}}{2b} > \delta_{ub} K.$$

Let

$$\theta_2 = \alpha(a - \Lambda - r_A \gamma_{ub}). \tag{24}$$

From condition (23), it follows that $\theta_2 > 0$. The Jacobian matrix evaluated at the real fixed point is

$$J_{21} = \begin{bmatrix} 1 + \frac{1}{2}\theta_2 + \alpha r_A(\gamma_{lb} + \gamma_{ub}) & 0 \\ -\frac{1}{2}\theta_2 & 1 - \theta_2 \end{bmatrix}.$$

The eigenvalues are

$$\lambda_1 = 1 + \frac{1}{2}\theta_2 + \alpha r_A(\gamma_{lb} + \gamma_{ub}) > 1 \quad \text{and} \quad \lambda_2 = 1 - \theta_2.$$

Therefore, $\mathbb{E}_{21}$ is unstable. In particular, when $\theta_2 < 2$, $\mathbb{E}_{21}$ is a saddle point.
We do not analyze border-collision bifurcations in this case, since the real fixed point of System 2 is never stable.
Next, System 4 has the following fixed points:

$$\mathbb{E}_{41} = \left(0, \frac{a - \Lambda + r_A \gamma_{lb}}{2b}\right), \quad \mathbb{E}_{42} = \left(\frac{a - \Lambda - r_A \gamma_{ub}}{2b}, 0\right), \quad \text{and}$$
$$\mathbb{E}_{43} = \left(\frac{a - \Lambda - r_A \gamma_{lb} - 2r_A \gamma_{ub}}{3b}, \frac{a - \Lambda + 2r_A \gamma_{lb} + r_A \gamma_{ub}}{3b}\right).$$

Recall the definition of the region Ω_4. The conditions defining Ω_4 imply that

$$L_2 < \delta_{lb} K < \delta_{ub} K < L_1.$$

Hence, $\mathbb{E}_{41}$ and $\mathbb{E}_{43}$ are always virtual fixed points, whereas $\mathbb{E}_{42}$ is a real fixed point if

$$\frac{a - \Lambda - r_A \gamma_{ub}}{2b} > \delta_{ub} K.$$

Similarly to the analysis of System 2, $\mathbb{E}_{42}$ is unstable, and it is a saddle point when $\theta_2 < 2$.

3.3. System 3 and System 7

The fixed points of System 3 are

$$\mathbb{E}_{31} = \left(0, \frac{a-\Lambda}{2b}\right), \quad \mathbb{E}_{32} = \left(\frac{a-\Lambda+r_A\gamma_{lb}}{2b}, 0\right), \quad \text{and}$$
$$\mathbb{E}_{33} = \left(\frac{a-\Lambda+2r_A\gamma_{lb}}{3b}, \frac{a-\Lambda-r_A\gamma_{lb}}{3b}\right).$$

The boundary equilibria have nonnegative coordinates, and the interior equilibrium has strictly positive coordinates, if

$$a > \Lambda + r_A\gamma_{lb}. \tag{25}$$

Recall the definition of the region Ω_3. The conditions defining Ω_3 imply that $L_1 < \delta_{lb}K \le L_2 < \delta_{ub}K$. Hence, $\mathbb{E}_{32}$ and $\mathbb{E}_{33}$ are always virtual fixed points, whereas $\mathbb{E}_{31}$ is a real fixed point if

$$\delta_{lb}K \le \frac{a-\Lambda}{2b} \le \delta_{ub}K.$$

Let

$$\theta_3 = \alpha(a-\Lambda). \tag{26}$$

From (25), it follows that $\theta_3 > 0$. The Jacobian matrix evaluated at the real fixed point is

$$J_{31} = \begin{bmatrix} 1+\frac{1}{2}\theta_3+\alpha r_A\gamma_{lb} & 0 \\ -\frac{1}{2}\theta_3 & 1-\theta_3 \end{bmatrix}.$$

The eigenvalues are

$$\lambda_1 = 1+\frac{1}{2}\theta_3+\alpha r_A\gamma_{lb} > 1, \qquad \lambda_2 = 1-\theta_3.$$

Therefore, $\mathbb{E}_{31}$ is unstable. In particular, it is a saddle point when $\theta_3 < 2$.
Next, System 7 has the following fixed points:

$$\mathbb{E}_{71} = \left(0, \frac{a-\Lambda+r_A\gamma_{lb}}{2b}\right), \quad \mathbb{E}_{72} = \left(\frac{a-\Lambda}{2b}, 0\right), \quad \text{and}$$
$$\mathbb{E}_{73} = \left(\frac{a-\Lambda-r_A\gamma_{lb}}{3b}, \frac{a-\Lambda+2r_A\gamma_{lb}}{3b}\right).$$

Recall the definition of the region Ω_7. The conditions defining Ω_7 imply that

$$L_2 < \delta_{lb}K \le L_1 < \delta_{ub}K.$$

Hence, $\mathbb{E}_{71}$ and $\mathbb{E}_{73}$ are always virtual fixed points, whereas $\mathbb{E}_{72}$ is a real fixed point if

$$\delta_{lb}K \le \frac{a-\Lambda}{2b} \le \delta_{ub}K.$$

Similarly to the analysis of System 3, $\mathbb{E}_{72}$ is unstable, and it is a saddle point when $\theta_3 < 2$.

3.4. System 5

The fixed points are

$$\mathbb{E}_{51} = \left(0, \frac{a-\Lambda-r_A\gamma_{ub}}{2b}\right), \quad \mathbb{E}_{52} = \left(\frac{a-\Lambda-r_A\gamma_{ub}}{2b}, 0\right), \quad \text{and}$$
$$\mathbb{E}_{53} = \left(\frac{a-\Lambda-r_A\gamma_{ub}}{3b}, \frac{a-\Lambda-r_A\gamma_{ub}}{3b}\right).$$

The boundary equilibria have nonnegative coordinates, and the interior equilibrium has strictly positive coordinates, if

$$a > \Lambda + r_A\gamma_{ub}. \tag{27}$$

Recall the definition of the region Ω_5. The conditions defining Ω_5 imply that

$$L_1 > \delta_{ub}K > 0, \qquad L_2 > \delta_{ub}K > 0.$$

Hence, $\mathbb{E}_{51}$ and $\mathbb{E}_{52}$ are always virtual fixed points, whereas $\mathbb{E}_{53}$ is a real fixed point if

$$\frac{a-\Lambda-r_A\gamma_{ub}}{3b} > \delta_{ub}K.$$

We have the following result concerning the stability of the real fixed point.

Theorem 3. *Let* $\frac{a-\Lambda-r_A\gamma_{ub}}{3b} > \delta_{ub}K$, *then*

$$\mathbb{E}_{53} = \left(\frac{a-\Lambda-r_A\gamma_{ub}}{3b}, \frac{a-\Lambda-r_A\gamma_{ub}}{3b}\right)$$

is locally asymptotically stable if

$$\gamma_{ub} > \frac{1}{\alpha r_A}[\alpha(a-\Lambda)-2].$$

Proof. From condition (27), we have $\theta_2 = \alpha(a-\Lambda-r_A\gamma_{ub}) > 0$ as defined in (24). The Jacobian matrix of System 5 evaluated at the real fixed point is

$$J_{53} = \begin{bmatrix} 1-\frac{2}{3}\theta_2 & -\frac{1}{3}\theta_2 \\ -\frac{1}{3}\theta_2 & 1-\frac{2}{3}\theta_2 \end{bmatrix}.$$

We have $\mathrm{tr}(J_{53}) = 2-\frac{4}{3}\theta_2$ and $\det(J_{53}) = 1-\frac{4}{3}\theta_2+\frac{1}{3}\theta_2^2$.

The Jury stability conditions are

$$F = 4-\frac{8}{3}\theta_2+\frac{1}{3}\theta_2^2 = \frac{1}{3}[(\theta_2-4)^2-4] > 0 \quad \text{if} \quad \theta_2 < 2 \text{ or } \theta_2 > 6,$$

$$T = \frac{1}{3}\theta_2^2 > 0,$$

$$N = \frac{4}{3}\theta_2-\frac{1}{3}\theta_2^2 > 0 \quad \text{if} \quad \theta_2 < 4.$$

These conditions hold if $\theta_2 < 2$, which is equivalent to

$$\gamma_{ub} > \frac{1}{\alpha r_A}[\alpha(a-\Lambda)-2]. \tag{28}$$

Therefore, $\mathbb{E}_{53}$ is locally asymptotically stable if condition (28) holds. □

The stable fixed point $\mathbb{E}_{53}$ may undergo a flip bifurcation when $\gamma_{ub} = \gamma_{ub}^F$, where

$$\gamma_{ub}^F = \frac{1}{\alpha r_A}[\alpha(a-\Lambda)-2].$$

Hence, $\mathbb{E}_{53}$ is stable if $\gamma_{ub} > \gamma_{ub}^F$.

Next, we study the border-collision bifurcation of $\mathbb{E}_{53} = (L_1^*, L_2^*)$. System 5 has borders $L_1 = \delta_{ub}K$ and $L_2 = \delta_{ub}K$. The fixed point $\mathbb{E}_{53}$ may undergo a border-collision bifurcation when

$$\frac{a-\Lambda-r_A\gamma_{ub}}{3b} = \delta_{ub}K.$$

This condition is equivalent to $\gamma_{ub} = \gamma_{ub}^B$, where

$$\gamma_{ub}^B = \frac{1}{r_A}[(a-\Lambda)-3b\delta_{ub}K],$$

or $\delta_{ub} = \delta_{ub}^{B_1}$, where

$$\delta_{ub}^{B_1} = \frac{a-\Lambda-r_A\gamma_{ub}}{3bK}.$$

In this case, $\mathbb{E}_{53}$ must satisfy

$$L_1^* > \delta_{ub}K, \qquad L_2^* > \delta_{ub}K,$$

that is,

$$\gamma_{ub} < \gamma_{ub}^B \quad \text{or} \quad \delta_{ub} < \delta_{ub}^{B_1}.$$

From this analysis, the stability conditions for $\mathbb{E}_{53}$ are

$$\gamma_{ub} > \gamma_{ub}^F, \qquad \gamma_{ub} < \gamma_{ub}^B.$$

Hence, if $\gamma_{ub}^F > \gamma_{ub}^B$, then $\mathbb{E}_{53}$ is never stable. Therefore, it must hold that $\gamma_{ub}^F < \gamma_{ub}^B$. The complete stability condition for $\mathbb{E}_{53}$ is

$$\gamma_{ub}^F < \gamma_{ub} < \gamma_{ub}^B.$$

Since $\gamma_{ub} > 0$, if $\gamma_{ub}^F < 0$, then the stability condition reduces to $\gamma_{ub} < \gamma_{ub}^B$. If $\gamma_{ub}^B < 0$, then $\mathbb{E}_{53}$ is never stable. These results are summarized in the following theorem.

Theorem 4. *Suppose* $\gamma_{ub}^B > 0$,

1. *if* $\gamma_{ub}^F > 0$, *then* $\mathbb{E}_{53}$ *is stable when* $\gamma_{ub}^F < \gamma_{ub} < \gamma_{ub}^B$. *It may undergo a flip bifurcation at* $\gamma_{ub} = \gamma_{ub}^F$ *and a border-collision bifurcation at* $\gamma_{ub} = \gamma_{ub}^B$;
2. *if* $\gamma_{ub}^F < 0$, *then* $\mathbb{E}_{53}$ *is stable when* $0 < \gamma_{ub} < \gamma_{ub}^B$. *It loses stability through a border-collision bifurcation at* $\gamma_{ub} = \gamma_{ub}^B$.

3.5. System 6 and System 8

The fixed points of System 6 are

$$\mathbb{E}_{61} = \left(0, \frac{a-\Lambda}{2b}\right), \quad \mathbb{E}_{62} = \left(\frac{a-\Lambda-r_A\gamma_{ub}}{2b}, 0\right), \quad \text{and}$$
$$\mathbb{E}_{63} = \left(\frac{a-\Lambda-2r_A\gamma_{ub}}{3b}, \frac{a-\Lambda+r_A\gamma_{ub}}{3b}\right).$$

The boundary equilibria have nonnegative coordinates, and the interior equilibrium has strictly positive coordinates, if

$$a > \Lambda + 2r_A\gamma_{ub}. \tag{29}$$

Recall the definition of the region Ω_6. The conditions defining Ω_6 imply that $0 < \delta_{lb}K \le L_2 \le \delta_{ub}K < L_1$. Hence, all the fixed points of System 6 are always virtual.

Next, System 8 has the following fixed points:

$$\mathbb{E}_{81} = \left(0, \frac{a-\Lambda-r_A\gamma_{ub}}{2b}\right), \quad \mathbb{E}_{82} = \left(\frac{a-\Lambda}{2b}, 0\right), \quad \text{and}$$
$$\mathbb{E}_{83} = \left(\frac{a-\Lambda+r_A\gamma_{ub}}{3b}, \frac{a-\Lambda-2r_A\gamma_{ub}}{3b}\right).$$

Recall the definition of the region Ω_8. The conditions defining Ω_8 imply that $0 < \delta_{lb}K \le L_1 \le \delta_{ub}K < L_2$. Hence, all the fixed points of System 8 are also always virtual.

Systems 6 and 8 do not generate real fixed points; therefore, no stability or smooth bifurcation analysis is required.

3.6. System 9

The fixed points are

$$\mathbb{E}_{91} = \left(0, \frac{a-\Lambda}{2b}\right), \quad \mathbb{E}_{92} = \left(\frac{a-\Lambda}{2b}, 0\right), \quad \text{and}$$
$$\mathbb{E}_{93} = \left(\frac{a-\Lambda}{3b}, \frac{a-\Lambda}{3b}\right).$$

The boundary equilibria E_{91} and E_{92} have nonnegative coordinates, and the interior equilibrium E_{93} has strictly positive coordinates, if

$$a > \Lambda. \tag{30}$$

Recall the definition of the region Ω_9. The conditions defining Ω_9 imply that

$$0 < \delta_{lb}K \le L_1 \le \delta_{ub}K, \qquad 0 < \delta_{lb}K \le L_2 \le \delta_{ub}K.$$

Hence, $\mathbb{E}_{91}$ and $\mathbb{E}_{92}$ are always virtual fixed points, whereas $\mathbb{E}_{93}$ is a real fixed point if

$$\delta_{lb}K \le \frac{a-\Lambda}{3b} \le \delta_{ub}K.$$

We have the following result concerning the stability of the real fixed point.

Theorem 5. *If* $\delta_{lb}K \le \frac{a-\Lambda}{3b} \le \delta_{ub}K$, *then*

$$\mathbb{E}_{93} = \left(\frac{a-\Lambda}{3b}, \frac{a-\Lambda}{3b}\right)$$

is locally asymptotically stable if

$$\alpha < \frac{2}{a-\Lambda}.$$

Proof. From condition (30), we have $\theta_3 = \alpha(a-\Lambda) > 0$ as defined in (26). The Jacobian matrix of System 9 evaluated at the real fixed point is

$$J_{93} = \begin{bmatrix} 1-\frac{2}{3}\theta_3 & -\frac{1}{3}\theta_3 \\ -\frac{1}{3}\theta_3 & 1-\frac{2}{3}\theta_3 \end{bmatrix}.$$

We have $\mathrm{tr}(J_{93}) = 2 - \frac{4}{3}\theta_3$ and $\det(J_{93}) = 1 - \frac{4}{3}\theta_3 + \frac{1}{3}\theta_3^2$.

The Jury stability conditions are

$$F = 4 - \frac{8}{3}\theta_3 + \frac{1}{3}\theta_3^2 = \frac{1}{3}[(\theta_3-4)^2 - 4] > 0 \quad \text{if} \quad \theta_3 < 2 \text{ or } \theta_3 > 6,$$
$$T = \frac{1}{3}\theta_3^2 > 0,$$

$$N = \frac{4}{3}\theta_3 - \frac{1}{3}\theta_3^2 > 0 \quad \text{if} \quad \theta_3 < 4.$$

These conditions hold if $\theta_3 < 2$, which is equivalent to

$$\alpha < \frac{2}{a - \Lambda}. \tag{31}$$

Therefore, $\mathbb{E}_{93}$ is locally asymptotically stable if condition (31) holds. □

For this system, we do not study the local bifurcations of the smooth map, since the stability condition (31) does not involve the LDR-RR parameters. However, we analyze the border-collision bifurcation, since System 9 has borders

$$L_1 = \delta_{lb}K, \quad L_1 = \delta_{ub}K, \qquad L_2 = \delta_{lb}K, \quad L_2 = \delta_{ub}K.$$

The fixed point $\mathbb{E}_{93}$ may undergo a border-collision bifurcation when

$$\frac{a - \Lambda}{3b} = \delta_{lb}K \quad \text{or} \quad \frac{a - \Lambda}{3b} = \delta_{ub}K.$$

These conditions are equivalent to

$$\delta_{lb} = \delta_{lb}^{B_2}, \qquad \delta_{ub} = \delta_{ub}^{B_2},$$

where

$$\delta_{lb}^{B_2} = \frac{a - \Lambda}{3bK}, \qquad \delta_{ub}^{B_2} = \frac{a - \Lambda}{3bK}.$$

Thus, $\mathbb{E}_{93}$ must satisfy

$$\delta_{lb}K \le L_1^* \le \delta_{ub}K, \qquad \delta_{lb}K \le L_2^* \le \delta_{ub}K,$$

that is,

$$\delta_{lb} \le \delta_{lb}^{B_2}, \qquad \delta_{ub} \ge \delta_{ub}^{B_2}.$$

Theorem 6. *Suppose that condition (31) holds.*

1. *The fixed point $\mathbb{E}_{93}$ is locally asymptotically stable if*

$$\delta_{lb} \le \delta_{lb}^{B_2} \quad \text{and} \quad \delta_{ub} \ge \delta_{ub}^{B_2}.$$

2. *If $\delta_{lb} = \delta_{lb}^{B_2}$ or $\delta_{ub} = \delta_{ub}^{B_2}$, then the fixed point $\mathbb{E}_{93}$ undergoes a border-collision bifurcation.*

The following remark completes the local bifurcation analysis.

Remark 1. For the three diagonal equilibria that may become locally asymptotically stable, namely $\mathbb{E}_{13}$, $\mathbb{E}_{53}$, and $\mathbb{E}_{93}$, the eigenvalues are real. More precisely, they can be written as

$$\lambda_{i,1} = 1 - \theta_i, \qquad \lambda_{i,2} = 1 - \frac{\theta_i}{3},$$

where

$$\theta_1 = \alpha(a - \Lambda + r_A\gamma_{lb}), \qquad \theta_5 = \alpha(a - \Lambda - r_A\gamma_{ub}), \qquad \theta_9 = \alpha(a - \Lambda).$$

Therefore, a Neimark–Sacker bifurcation cannot occur at these equilibria, since such a bifurcation requires a complex conjugate pair of eigenvalues crossing the unit circle. The local stability conditions reduce to

$$|1 - \theta_i| < 1, \qquad \left|1 - \frac{\theta_i}{3}\right| < 1,$$

which, for positive θ_i, are equivalent to

$$0 < \theta_i < 2.$$

Thus, the relevant smooth loss of stability occurs when $\theta_i = 2$, so that $\lambda_{i,1} = -1$, corresponding to a flip (period-doubling) bifurcation, provided the usual nondegeneracy conditions hold. The condition associated with an eigenvalue $+1$ would require $\theta_i = 0$, and therefore does not define the stability boundary of the positive diagonal equilibria considered here. In addition to this smooth mechanism, nonsmooth transitions may occur when a fixed point crosses one of the switching boundaries and changes its real/virtual status, giving rise to a border-collision bifurcation.

In summary, the existence and stability of real fixed points strongly depend on the region in which the system operates and on the parameters of the LDR-RR mechanism. System 1 admits a stable interior fixed point $\mathbb{E}_{13}$ under suitable conditions on γ_{lb}, which may lose stability through a flip or border-collision bifurcation. System 5 exhibits a symmetric behavior with respect to the upper regulatory parameter γ_{ub}, where the fixed point $\mathbb{E}_{53}$ may lose stability through the same mechanisms. Systems 2, 3, 4, and 7

admit real fixed points that are always unstable, typically appearing as saddle points. Therefore, no stability region exists for these systems. Systems 6 and 8 do not generate any real fixed points, since all equilibrium points lie outside the corresponding regions. Finally, System 9 admits a symmetric interior equilibrium $\mathbb{E}_{93}$, whose stability depends on the adjustment parameter α and on the border parameters δ_{lb} and δ_{ub}. In this case, instability may arise through border-collision bifurcations.

Overall, the dynamics of the model are mainly governed by the interaction between the adjustment speed parameter α and the regulatory parameters γ_{lb}, γ_{ub}, δ_{lb}, and δ_{ub}, which determine both the existence and the stability of economically meaningful equilibria.

4. Virtual fixed points

Notice that all the obtained fixed points have nonnegative coordinates, and the interior equilibria have strictly positive coordinates, if

$$a > \Lambda + r_A\gamma_{lb} + 2r_A\gamma_{ub}. \tag{32}$$

Some of the fixed points obtained from Systems 1–9 coincide, although they may have different classifications as real or virtual. The classification of fixed points as real or virtual depends on the region in which the system operates. Our classifications are summarized in Table 2.

In piecewise dynamical systems, virtual fixed points may still influence the global dynamics even though they do not belong to the active region. Let $i = 1, 2, \ldots, 9$, $F_i : \Omega_i \to \mathbb{R}^2$ denote the local map associated with System S_i, and let $\mathbb{E}_i$ satisfy

$$F_i(\mathbb{E}_i) = \mathbb{E}_i.$$

If $\mathbb{E}_i \notin \Omega_i$, then $\mathbb{E}_i$ is a virtual fixed point. Nevertheless, for every initial condition $(L_{1,t}, L_{2,t}) \in \Omega_i$, the iterate $F_i(L_{1,t}, L_{2,t})$ is still governed by the same local map whose fixed point is $\mathbb{E}_i$. Hence, although a trajectory cannot converge to a virtual fixed point while remaining in Ω_i, the local evolution is still influenced by the corresponding subsystem until the orbit reaches a switching boundary.

Moreover, the coordinates of the fixed points depend continuously on the model parameters. Hence, when a parameter varies, a fixed point generated by a local subsystem may cross one of the switching boundaries and change from virtual to real, or vice versa. In the present model, this mechanism is especially relevant for the three diagonal equilibria that may become locally stable. The lower-regime equilibrium $\mathbb{E}_{13}$ crosses the lower switching boundary when

$$\frac{a - \Lambda + r_A\gamma_{lb}}{3b} = \delta_{lb}K,$$

while the upper-regime equilibrium $\mathbb{E}_{53}$ crosses the upper switching boundary when

$$\frac{a - \Lambda - r_A\gamma_{ub}}{3b} = \delta_{ub}K.$$

Similarly, the central equilibrium $\mathbb{E}_{93}$ becomes real only when it lies inside the regulatory corridor,

$$\delta_{lb}K \le \frac{a - \Lambda}{3b} \le \delta_{ub}K.$$

These crossings correspond to changes in the real/virtual status of the relevant equilibrium and therefore produce border-collision transitions. Thus, the abrupt transitions observed in the numerical diagrams when γ_{lb}, γ_{ub}, δ_{lb}, or δ_{ub} vary can be interpreted as the dynamical effect of virtual fixed points becoming admissible, or real fixed points becoming virtual, at the corresponding switching boundaries.

Table 2 highlights that only three interior equilibria, $\mathbb{E}_{13}$, $\mathbb{E}_{53}$, and $\mathbb{E}_{93}$, can become real fixed points, depending on the region in which the system operates, but they cannot be real simultaneously. The fixed points $\mathbb{E}_{23}$, $\mathbb{E}_{33}$, $\mathbb{E}_{43}$, $\mathbb{E}_{63}$, $\mathbb{E}_{73}$, and $\mathbb{E}_{83}$ are always virtual and never become real fixed points in any region.

Consider the following facts:

$$\delta_{lb} < \delta_{ub} \quad \text{and} \quad \frac{a - \Lambda - r_A\gamma_{ub}}{3b} < \frac{a - \Lambda}{3b} < \frac{a - \Lambda + r_A\gamma_{lb}}{3b}. \tag{33}$$

Recall that $\mathbb{E}_{13}$ is real if

$$\frac{a - \Lambda + r_A\gamma_{lb}}{3b} < \delta_{lb}K,$$

$\mathbb{E}_{53}$ is real if

$$\frac{a - \Lambda - r_A\gamma_{ub}}{3b} > \delta_{ub}K,$$

and $\mathbb{E}_{93}$ is real if

$$\delta_{lb}K \le \frac{a - \Lambda}{3b} \le \delta_{ub}K.$$

These observations lead to the following remarks.

Remark 2. The following properties hold:

Table 2
Distinct fixed points and their classification as real (R) or virtual (V) in Systems 1–9.

Fixed point	S1	S2	S3	S4	S5	S6	S7	S8	S9
$\mathbb{E}_{10} = (0,0)$	R	–	–	–	–	–	–	–	–
$\mathbb{E}_{11} = \mathbb{E}_{41} = \mathbb{E}_{71} = \left(0, \frac{a-\Lambda+r_A\gamma_{lb}}{2b}\right)$	R	–	–	V	–	–	V	–	–
$\mathbb{E}_{12} = \mathbb{E}_{22} = \mathbb{E}_{32} = \left(\frac{a-\Lambda+r_A\gamma_{lb}}{2b}, 0\right)$	R	V	V	–	–	–	–	–	–
$\mathbb{E}_{13} = \left(\frac{a-\Lambda+r_A\gamma_{lb}}{3b}, \frac{a-\Lambda+r_A\gamma_{lb}}{3b}\right)$	R	–	–	–	–	–	–	–	–
$\mathbb{E}_{21} = \mathbb{E}_{51} = \mathbb{E}_{81} = \left(0, \frac{a-\Lambda-r_A\gamma_{ub}}{2b}\right)$	–	R	–	–	V	–	–	V	–
$\mathbb{E}_{23} = \left(\frac{a-\Lambda+2r_A\gamma_{lb}+r_A\gamma_{ub}}{3b}, \frac{a-\Lambda-r_A\gamma_{lb}-2r_A\gamma_{ub}}{3b}\right)$	–	V	–	–	–	–	–	–	–
$\mathbb{E}_{31} = \mathbb{E}_{61} = \mathbb{E}_{91} = \left(0, \frac{a-\Lambda}{2b}\right)$	–	–	R	–	–	V	–	–	V
$\mathbb{E}_{33} = \left(\frac{a-\Lambda+2r_A\gamma_{lb}}{3b}, \frac{a-\Lambda-r_A\gamma_{lb}}{3b}\right)$	–	–	V	–	–	–	–	–	–
$\mathbb{E}_{42} = \mathbb{E}_{52} = \mathbb{E}_{62} = \left(\frac{a-\Lambda-r_A\gamma_{ub}}{2b}, 0\right)$	–	–	–	R	V	V	–	–	–
$\mathbb{E}_{43} = \left(\frac{a-\Lambda-r_A\gamma_{lb}-2r_A\gamma_{ub}}{3b}, \frac{a-\Lambda+2r_A\gamma_{lb}+r_A\gamma_{ub}}{3b}\right)$	–	–	–	V	–	–	–	–	–
$\mathbb{E}_{53} = \left(\frac{a-\Lambda-r_A\gamma_{ub}}{3b}, \frac{a-\Lambda-r_A\gamma_{ub}}{3b}\right)$	–	–	–	–	R	–	–	–	–
$\mathbb{E}_{63} = \left(\frac{a-\Lambda-2r_A\gamma_{ub}}{3b}, \frac{a-\Lambda+r_A\gamma_{ub}}{3b}\right)$	–	–	–	–	–	V	–	–	–
$\mathbb{E}_{72} = \mathbb{E}_{82} = \mathbb{E}_{92} = \left(\frac{a-\Lambda}{2b}, 0\right)$	–	–	–	–	–	–	R	V	V
$\mathbb{E}_{73} = \left(\frac{a-\Lambda-r_A\gamma_{lb}}{3b}, \frac{a-\Lambda+2r_A\gamma_{lb}}{3b}\right)$	–	–	–	–	–	–	V	–	–
$\mathbb{E}_{83} = \left(\frac{a-\Lambda+r_A\gamma_{ub}}{3b}, \frac{a-\Lambda-2r_A\gamma_{ub}}{3b}\right)$	–	–	–	–	–	–	–	V	–
$\mathbb{E}_{93} = \left(\frac{a-\Lambda}{3b}, \frac{a-\Lambda}{3b}\right)$	–	–	–	–	–	–	–	–	R

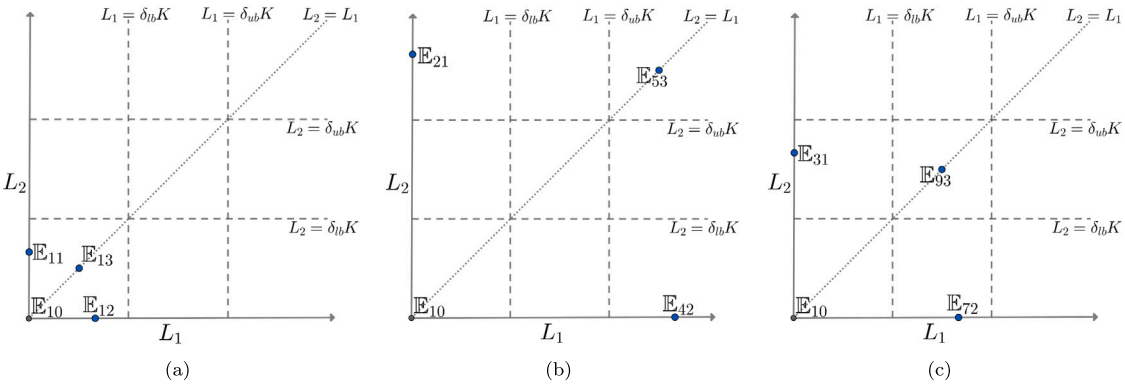


Fig. 3. The real fixed points of our systems.

1. If $\mathbb{E}_{13} = \left(\frac{a-\Lambda+r_A\gamma_{lb}}{3b}, \frac{a-\Lambda+r_A\gamma_{lb}}{3b}\right)$ is real, then $\mathbb{E}_{53}$ and $\mathbb{E}_{93}$ are virtual.
2. If $\mathbb{E}_{53} = \left(\frac{a-\Lambda-r_A\gamma_{ub}}{3b}, \frac{a-\Lambda-r_A\gamma_{ub}}{3b}\right)$ is real, then $\mathbb{E}_{13}$ and $\mathbb{E}_{93}$ are virtual.
3. If $\mathbb{E}_{93} = \left(\frac{a-\Lambda}{3b}, \frac{a-\Lambda}{3b}\right)$ is real, then $\mathbb{E}_{13}$ and $\mathbb{E}_{53}$ are virtual.

Thus, the three diagonal fixed points $\mathbb{E}_{13}$, $\mathbb{E}_{53}$, and $\mathbb{E}_{93}$ cannot be real simultaneously.

Note that Systems 6 and 8 never admit real fixed points; all their fixed points are always virtual.

Based on Remarks 2, the real fixed points are illustrated in Fig. 3. Among real fixed points, only the diagonal equilibria E_{13}, E_{53}, E_{93} can be locally asymptotically stable, under suitable parameter conditions. The boundary equilibria located on the coordinate axes are always unstable. Virtual fixed points, by definition, lie outside their defining regions and cannot be observed in actual dynamics.

5. Existence conditions of the bifurcations

This section provides analytical conditions for the existence of flip and border-collision bifurcations in the piecewise system. To avoid mixing different concepts, Table 3 separates the admissibility conditions, local stability conditions, and bifurcation conditions for the fixed points that may become locally stable.

Observe that the flip thresholds satisfy

$$\gamma_{lb}^F = \frac{2-\alpha(a-\Lambda)}{\alpha r_A}, \qquad \gamma_{ub}^F = \frac{\alpha(a-\Lambda)-2}{\alpha r_A},$$

Table 3
Admissibility, stability, and bifurcation conditions for the relevant fixed points. Here BCB stands for border-collision bifurcation.

Fixed point	Admissibility	Local stability	Stability loss
$\mathbb{E}_{13}$	$\delta_{lb} > \frac{a-\Lambda+r_A\gamma_{lb}}{3bK}$	$\theta_1 < 2$	Flip if $\theta_1 = 2$; BCB if $\delta_{lb} = \frac{a-\Lambda+r_A\gamma_{lb}}{3bK}$
$\mathbb{E}_{53}$	$\delta_{ub} < \frac{a-\Lambda-r_A\gamma_{ub}}{3bK}$	$\theta_2 < 2$	Flip if $\theta_2 = 2$; BCB if $\delta_{ub} = \frac{a-\Lambda-r_A\gamma_{ub}}{3bK}$
$\mathbb{E}_{93}$	$\delta_{lb} \le \frac{a-\Lambda}{3bK} \le \delta_{ub}$	$\theta_3 < 2$	Flip if $\theta_3 = 2$; BCB if $\delta_{lb} = \frac{a-\Lambda}{3bK}$ or $\delta_{ub} = \frac{a-\Lambda}{3bK}$

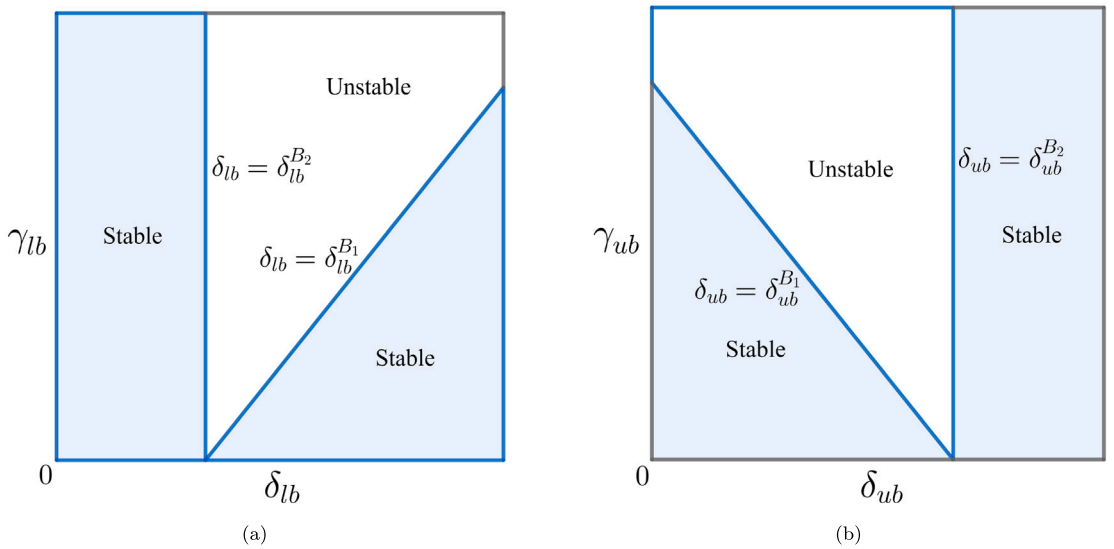


Fig. 4. Stability regions in the policy-parameter planes: (a) lower-side penalty coefficient γ_{lb} and lower LDR bound δ_{lb}; (b) upper-side penalty coefficient γ_{ub} and upper LDR bound δ_{ub}. The shaded regions identify parameter combinations for which the corresponding equilibrium remains locally stable and admissible.

so that $\gamma_{lb}^F = -\gamma_{ub}^F$. By contrast, for the border-collision thresholds:

$$\gamma_{lb}^B = \frac{3b\delta_{lb}K - (a-\Lambda)}{r_A}, \qquad \gamma_{ub}^B = \frac{(a-\Lambda) - 3b\delta_{ub}K}{r_A},$$

one has $\gamma_{lb}^B + \gamma_{ub}^B = \frac{3bK(\delta_{lb}-\delta_{ub})}{r_A} \neq 0$, since $\delta_{lb} < \delta_{ub}$.

The flip bifurcation values γ_{lb}^F and γ_{ub}^F do not depend on the parameters δ_{lb} and δ_{ub}. However, γ_{lb} and γ_{ub} determine the existence of the border-collision bifurcations associated with δ_{lb} and δ_{ub}.

In particular, γ_{lb}^B is a linear function of δ_{lb} with a positive slope, whereas γ_{ub}^B is a linear function of δ_{ub} with a negative slope. Conversely, $\delta_{lb}^{B_1}$ is a linear function of γ_{lb} with a positive slope, while $\delta_{ub}^{B_1}$ is a linear function of γ_{ub} with a negative slope.

To illustrate these relationships, Fig. 4 shows the stability regions of the systems in the two-parameter planes $(\gamma_{lb}, \delta_{lb})$ and $(\gamma_{ub}, \delta_{ub})$.

Fig. 4 translates the analytical stability conditions into two policy-oriented stability maps. Panel (a) focuses on the lower-side LDR-RR mechanism and shows how the stability region changes when the lower penalty coefficient γ_{lb} and the lower LDR bound δ_{lb} vary jointly. Panel (b) provides the analogous information for the upper-side mechanism, where the relevant policy parameters are the upper penalty coefficient γ_{ub} and the upper LDR bound δ_{ub}. These diagrams can be read as "safe zones" in the regulatory parameter space: inside the shaded regions, the corresponding equilibrium is both admissible and locally stable, whereas outside these regions the system either loses admissibility through a border-collision mechanism or loses local stability through a flip bifurcation. From a policy perspective, the maps show that changing the LDR corridor bounds modifies the admissible range of penalty coefficients. Therefore, the penalty parameters γ_{lb} and γ_{ub} should not be calibrated independently of the corridor thresholds δ_{lb} and δ_{ub}.

Fig. 5 complements the analytical stability maps by showing how the attracting dynamics changes when the two penalty coefficients vary jointly. The period-one regions identify combinations of $(\gamma_{lb}, \gamma_{ub})$ for which trajectories converge to a fixed point and can therefore be interpreted as numerical safe zones. Panel (a) shows that, in the lower-side scenario, the transition away from period-one dynamics is mainly organized by the lower penalty coefficient γ_{lb}, as indicated by the vertical structure around the border-collision threshold γ_{lb}^B. Panel (b) shows the analogous upper-side scenario, where the transition is mainly governed by the upper penalty coefficient γ_{ub} and occurs around the threshold γ_{ub}^B. Thus, the joint calibration of the lower- and upper-side penalty coefficients affects the stability of lending dynamics, but the dominant destabilizing direction depends on which side of the LDR-RR mechanism is active.

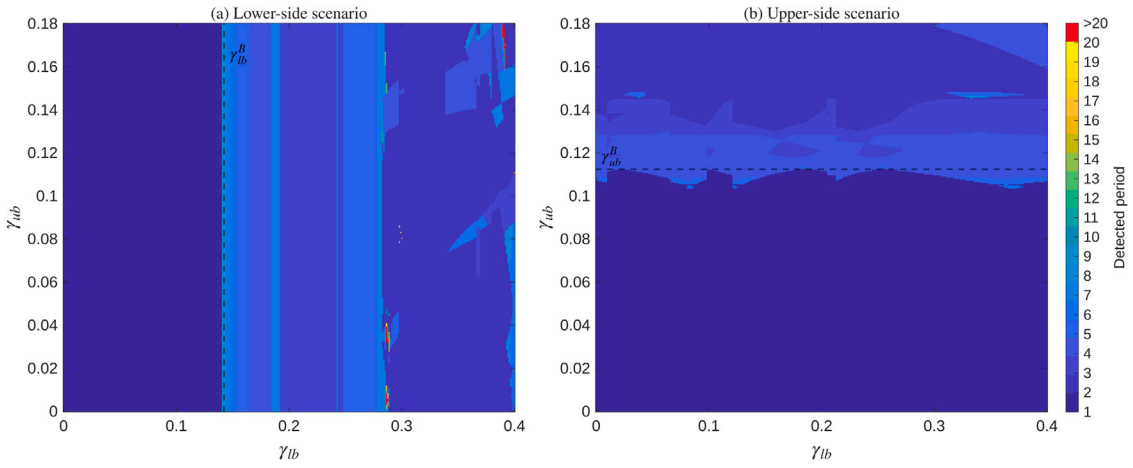


Fig. 5. Numerical two-parameter maps in the $(\gamma_{lb}, \gamma_{ub})$ plane. The color bar denotes the detected period of the attracting set, while the period-one region can be interpreted as a numerical safe zone. Panel (a) refers to the lower-side scenario and uses $\alpha = 25$ and $a = 0.135$; panel (b) refers to the upper-side scenario and uses $\alpha = 30$ and $a = 0.16$. Common parameters are $b = 0.07$, $r_A = 0.08$, $K = 0.1$, $\Lambda = 0.13$, $\delta_{lb} = 0.78$, $\delta_{ub} = 1$, $L_{1,0} = 0.02$, and $L_{2,0} = 0.01$. The dashed lines denote the corresponding border-collision thresholds predicted by the analytical conditions.

There are six bifurcation scenarios with respect to the LDR-RR parameters that may occur: two flip bifurcations and four border-collision bifurcations. In the next section, their occurrence will be illustrated through numerical simulations using bifurcation diagrams of the LDR-RR parameters. Before presenting the simulations, we derive the conditions under which each bifurcation can occur.

First, the flip bifurcation value γ_{lb}^F exists if

$$\gamma_{lb}^F > 0 \quad \text{and} \quad \gamma_{lb}^F < \gamma_{lb}^B.$$

The condition $\gamma_{lb}^F > 0$ implies $\alpha < \frac{2}{a-\Lambda}$, while the condition $\gamma_{lb}^F < \gamma_{lb}^B$ implies $\alpha > \frac{2}{3b\delta_{lb}K}$. Combining these two conditions yields the existence condition for γ_{lb}^F:

$$\frac{2}{3b\delta_{lb}K} < \alpha < \frac{2}{a-\Lambda}. \tag{34}$$

Next, the border-collision bifurcation value γ_{lb}^B exists if

$$\gamma_{lb}^B > 0 \quad \text{and} \quad \gamma_{lb}^B < \gamma_{lb}^F.$$

The condition $\gamma_{lb}^B > 0$ implies $\delta_{lb} > \frac{a-\Lambda}{3bK}$, while $\gamma_{lb}^B < \gamma_{lb}^F$ implies $\delta_{lb} < \frac{2}{3\alpha bK}$. Combining these conditions gives the existence condition for γ_{lb}^B:

$$\frac{a-\Lambda}{3bK} < \delta_{lb} < \frac{2}{3\alpha bK}. \tag{35}$$

Furthermore, the bifurcation values γ_{ub}^F and γ_{ub}^B both exist if

$$\gamma_{ub}^F > 0 \quad \text{and} \quad \gamma_{ub}^F < \gamma_{ub}^B.$$

The condition $\gamma_{ub}^F > 0$ implies $\alpha > \frac{2}{a-\Lambda}$, while $\gamma_{ub}^F < \gamma_{ub}^B$ implies $\alpha < \frac{2}{3b\delta_{ub}K}$. Therefore, the existence condition for γ_{ub}^F and γ_{ub}^B is

$$\frac{2}{a-\Lambda} < \alpha < \frac{2}{3b\delta_{ub}K}. \tag{36}$$

Only the border-collision bifurcation γ_{ub}^B exists (i.e., γ_{ub}^F does not exist) if

$$\gamma_{ub}^B > 0 \quad \text{and} \quad \gamma_{ub}^F < 0.$$

The condition $\gamma_{ub}^B > 0$ implies $\delta_{ub} < \frac{a-\Lambda}{3bK}$, while $\gamma_{ub}^F < 0$ implies $\alpha < \frac{2}{a-\Lambda}$. Hence, the existence condition for γ_{ub}^B only is

$$\delta_{ub} < \frac{a-\Lambda}{3bK}, \qquad \alpha < \frac{2}{a-\Lambda}. \tag{37}$$

Recall that $\delta_{lb} < \delta_{ub}$ and Condition (32) holds. Consequently, $\delta_{lb}^{B_1}$, $\delta_{lb}^{B_2}$, $\delta_{ub}^{B_1}$, and $\delta_{ub}^{B_2}$ are all positive. Moreover, we have $\delta_{lb}^{B_2} < \delta_{lb}^{B_1}$ and $\delta_{ub}^{B_1} < \delta_{ub}^{B_2}$. Their existence conditions are given as follows:

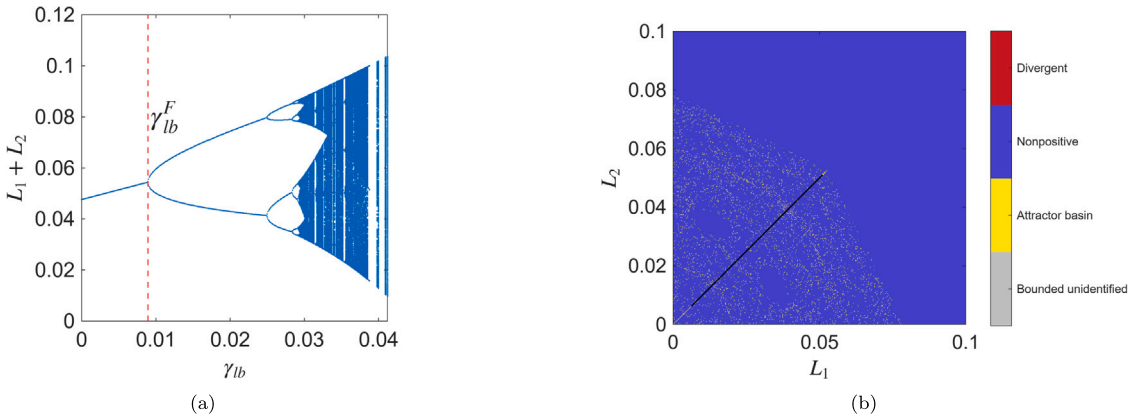


Fig. 6. Economic scenario 1. (a) Bifurcation diagram with respect to γ_{lb}, where $L^* = L_1^* + L_2^*$, when the stable equilibrium loses stability through a flip bifurcation. The simulation uses $\alpha = 350$, $a = 0.135$, $b = 0.07$, $r_A = 0.08$, $K = 0.1$, $\Lambda = 0.13$, $\delta_{lb} = 0.78$, $\delta_{ub} = 1$, $\gamma_{ub} = 0.2$, $L_{1,0} = 0.02$, and $L_{2,0} = 0.01$. (b) Basin diagram for $\gamma_{lb} = 0.04$. Yellow denotes the basin of the displayed attracting set, gray denotes bounded but unidentified initial conditions, blue denotes trajectories leaving the positive quadrant, and red denotes divergent or nonfinite trajectories. Black points represent the displayed attracting set.

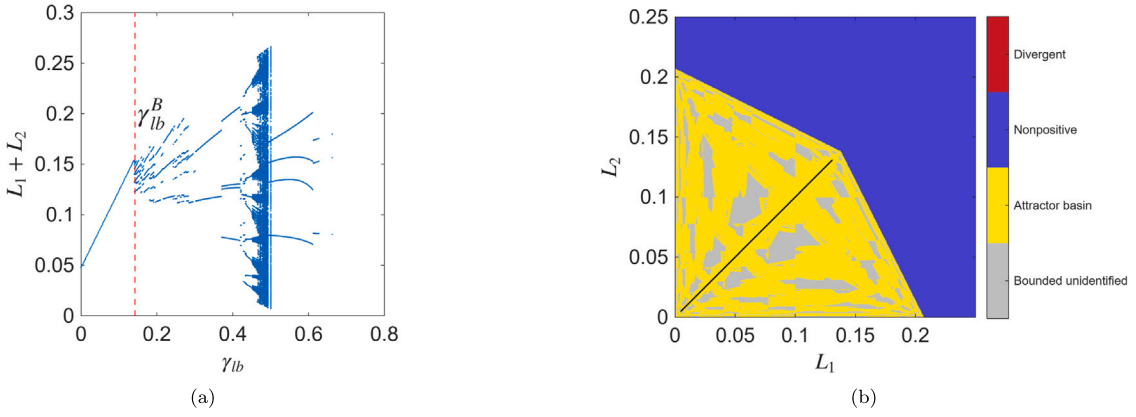


Fig. 7. Economic scenario 2. (a) Bifurcation diagram with respect to γ_{lb}, where $L^* = L_1^* + L_2^*$, when a border-collision bifurcation occurs. The simulation uses $\alpha = 25$, $a = 0.135$, $b = 0.07$, $r_A = 0.08$, $K = 0.1$, $\Lambda = 0.13$, $\delta_{lb} = 0.78$, $\delta_{ub} = 1$, $\gamma_{ub} = 0.2$, $L_{1,0} = 0.02$, and $L_{2,0} = 0.01$. (b) Basin diagram for $\gamma_{lb} = 0.48$. Yellow denotes the basin of the displayed attracting set, gray denotes bounded but unidentified initial conditions, blue denotes trajectories leaving the positive quadrant, and red denotes divergent or nonfinite trajectories. Black points represent the displayed attracting set.

(a) $\delta_{lb}^{B_1}$ exists if

$$\delta_{lb}^{B_1} < \delta_{ub} \quad \Leftrightarrow \quad \delta_{ub} > \frac{a - \Lambda + r_A \gamma_{lb}}{3bK}. \tag{38}$$

(b) $\delta_{lb}^{B_2}$ always exists.

(c) $\delta_{ub}^{B_1}$ exists if

$$\delta_{lb} < \delta_{ub}^{B_1} \quad \Leftrightarrow \quad \delta_{lb} < \frac{a - \Lambda - r_A \gamma_{ub}}{3bK}. \tag{39}$$

(d) $\delta_{ub}^{B_2}$ always exists.

6. Simulations

6.1. Economic scenario

All numerical simulations reported in Figs. 6–12 were recomputed using explicit positivity, boundedness, and divergence checks. All computations were performed in MATLAB using IEEE 754 double-precision floating-point arithmetic. For the one-parameter

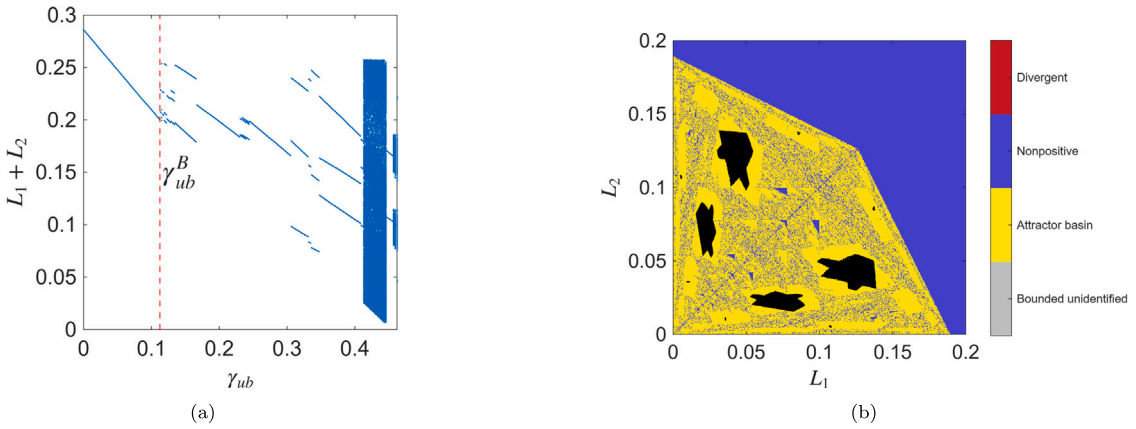


Fig. 8. Economic scenario 3. (a) Bifurcation diagram with respect to γ_{ub}, where $L^* = L_1^* + L_2^*$, when a border-collision bifurcation occurs. The simulation uses $\alpha = 30$, $a = 0.16$, $b = 0.07$, $r_A = 0.08$, $K = 0.1$, $\Lambda = 0.13$, $\delta_{lb} = 0.78$, $\delta_{ub} = 1$, $\gamma_{lb} = 0.1$, $L_{1,0} = 0.02$, and $L_{2,0} = 0.01$. (b) Basin diagram for $\gamma_{ub} = 0.46$. Yellow denotes the basin of the displayed attracting set, gray denotes bounded but unidentified initial conditions, blue denotes trajectories leaving the positive quadrant, and red denotes divergent or nonfinite trajectories. Black points represent the displayed attracting set.

bifurcation diagrams, the first 5000 iterations were discarded as transients and the following 1000 iterations were plotted, giving a total of 6000 iterations for each parameter value. Each parameter interval was discretized into 501 equally spaced values.

For the basin diagrams, the phase space was discretized by using a 500 × 500 grid of initial conditions. Each initial condition was iterated for 5000 transient steps followed by 1000 classification steps. The reference attracting set was computed over a longer orbit, discarding the initial transient, and was represented on a finite occupancy grid. During the classification stage, each surviving trajectory was compared with this reference set. Initial conditions whose post-transient iterates matched the reference attracting set according to the adopted finite-time criterion were classified as belonging to its basin. Trajectories that remained positive, finite, and below the divergence threshold but did not satisfy this matching criterion were classified as bounded but unidentified.

For the two-parameter isoperiodic diagrams, periods up to 20 were tested using the full two-dimensional state (L_1, L_2), with tolerance 10^{-8}. The parameter planes in Figs. 12(a)–12(c) were discretized by using a 200 × 200 grid, whereas Fig. 12(d) was computed on a 500 × 500 grid. The final periodic block was compared with preceding repetitions in order to reduce false period identification. At every iteration, trajectories were checked for positivity, finite numerical values, and divergence. A trajectory was classified as nonpositive when $L_1 < 0$ or $L_2 < 0$, and as divergent when $\max\{|L_1|, |L_2|\} > 1$ or when nonfinite numerical values occurred. Only trajectories that remained positive, finite, and below the divergence threshold throughout the prescribed numerical horizon were classified as economically meaningful asymptotic dynamics.

To complement the local analysis developed in the previous sections, we now investigate the global dynamics of map S by means of numerical simulations. In all one-parameter diagrams, we plot the asymptotic value of total loans, $L^* = L_1^* + L_2^*$, after discarding a sufficiently long transient. The aim is to illustrate the bifurcation scenarios predicted by the analytical thresholds derived in Section 5 and to show how the global attractors change when the regulatory parameters vary. Since the simulations are performed from fixed initial conditions, the diagrams track the attractor selected by those initial conditions and may therefore reveal coexistence phenomena when multiple attractors are present.

Fig. 6 illustrates the case in which the lower-side penalty parameter γ_{lb} gives rise to a flip bifurcation. For the parameter values used in Fig. 6(a), the theoretical threshold γ_{lb}^F exists and lies inside the displayed interval, whereas the border-collision value γ_{lb}^B is located farther to the right. Accordingly, the diagram shows a smooth loss of stability at the predicted value of γ_{lb}^F, followed by oscillatory behavior and a period-doubling route to chaos. The basin plot in Fig. 6(b) confirms that, after the local instability sets in, the long-run dynamics is governed by a nontrivial attractor with a highly structured basin.

A different situation is shown in Fig. 7. Here the relevant threshold is the border-collision value γ_{lb}^B, which is reached before the flip condition becomes active. As a consequence, the bifurcation diagram in Fig. 7(a) displays an abrupt transition when the attractor collides with the switching boundary. For larger values of γ_{lb}, the dynamics becomes irregular and the basin shown in Fig. 7(b) highlights the global nature of the transition. Therefore, Figs. 6 and 7 provide two complementary examples for the lower regulatory parameter: depending on the value of α, instability may emerge either through a smooth flip bifurcation or through a nonsmooth border-collision bifurcation.

The role of the upper-side penalty parameter γ_{ub} is illustrated in Figs. 8 and 9. In Fig. 8, the parameter configuration implies that only the border-collision threshold is relevant. Consistently with the analytical predictions, the attractor remains regular up to the theoretical value γ_{ub}^B, while for larger values of γ_{ub} the dynamics becomes irregular. The basin reported in Fig. 8(b) shows that the upper border may also generate a complicated global organization of the phase space.

Fig. 9 corresponds to a parameter set for which both the flip and the border-collision thresholds exist and are visible in the explored parameter window. The first loss of stability occurs at γ_{ub}^F, where the stable fixed point undergoes a flip bifurcation, while the second transition takes place at γ_{ub}^B, where the attractor collides with the switching boundary. The basin plot shown in panel

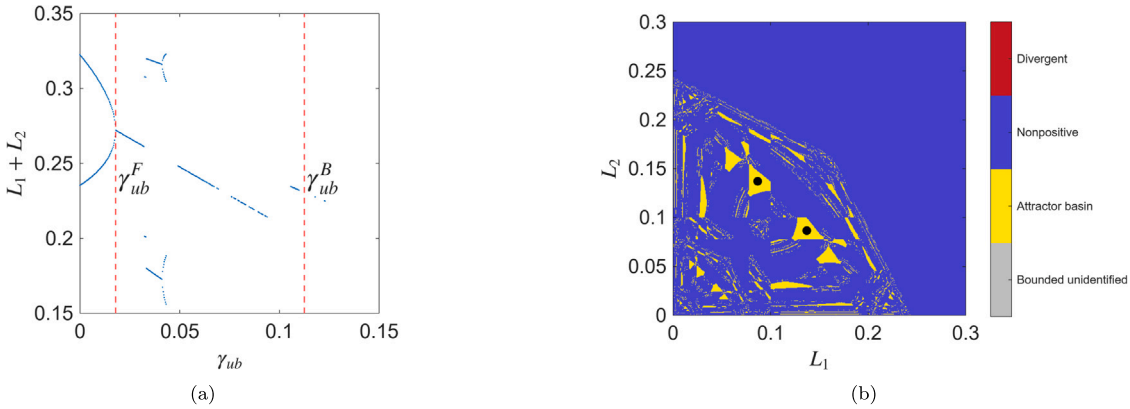


Fig. 9. Economic scenario 4. (a) Bifurcation diagram with respect to γ_{ub}, where $L^* = L_1^* + L_2^*$, when both flip and border-collision thresholds are relevant. The simulation uses $\alpha = 70$, $a = 0.16$, $b = 0.07$, $r_A = 0.08$, $K = 0.1$, $\Lambda = 0.13$, $\delta_{lb} = 0.78$, $\delta_{ub} = 1$, $\gamma_{lb} = 0.1$, $L_{1,0} = 0.02$, and $L_{2,0} = 0.01$. The dashed vertical lines indicate the thresholds γ^F_{ub} and γ^B_{ub}. (b) Basin diagram for $\gamma_{ub} = 0.125$. Yellow denotes the basin of the displayed attracting set, gray denotes bounded but unidentified initial conditions, blue denotes trajectories leaving the positive quadrant, and red denotes divergent or nonfinite trajectories. Black points represent the displayed attracting set.

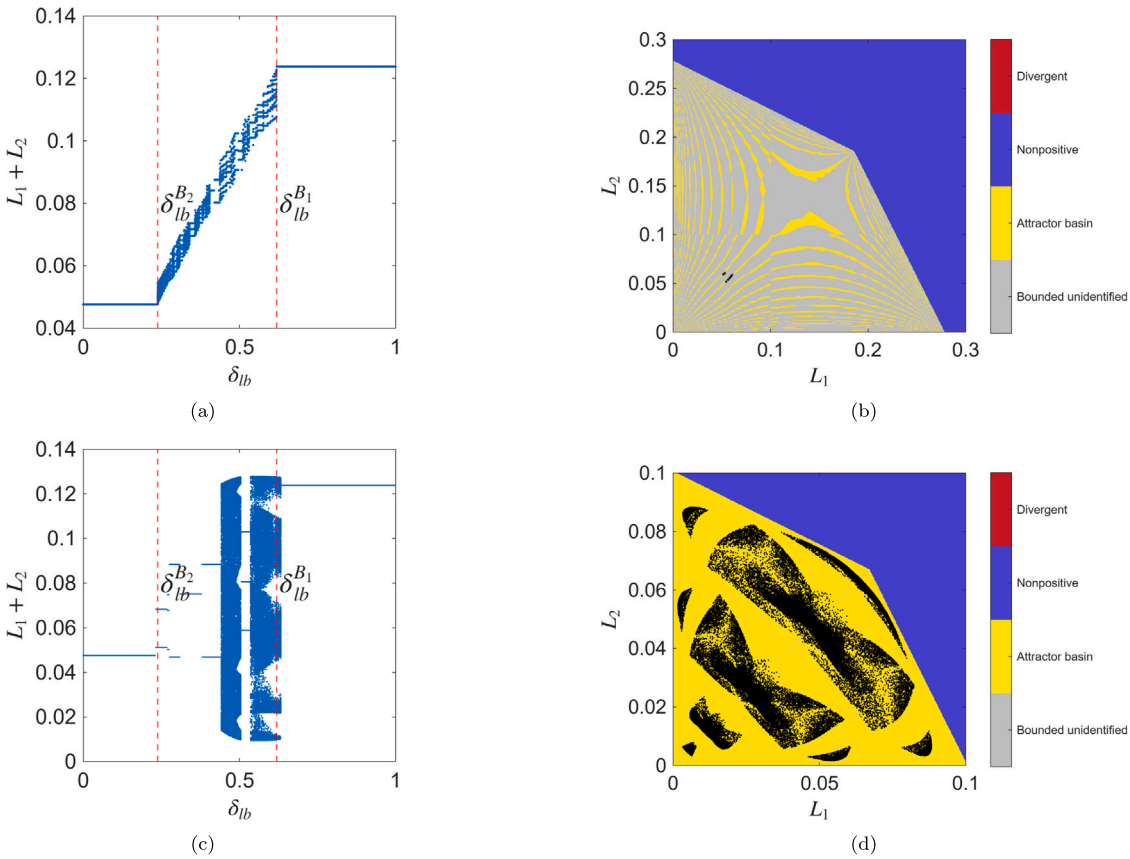


Fig. 10. Economic scenario 5. (a) Bifurcation diagram with respect to δ_{lb}, where $L^* = L_1^* + L_2^*$, when two border-collision bifurcations occur. The simulation uses $\alpha = 20$, $a = 0.135$, $b = 0.07$, $r_A = 0.08$, $K = 0.1$, $\Lambda = 0.13$, $\gamma_{lb} = 0.1$, $\gamma_{ub} = 0.2$, $\delta_{ub} = 1$, $L_{1,0} = 0.02$, and $L_{2,0} = 0.01$. (b) Basin diagram for $\delta_{lb} = 0.6$. (c) Bifurcation diagram with respect to δ_{lb} with $\alpha = 110$ and the remaining parameters unchanged. (d) Basin diagram for $\delta_{lb} = 0.6$ and $\alpha = 110$. In the basin diagrams, yellow denotes the basin of the displayed attracting set, gray denotes bounded but unidentified initial conditions, blue denotes trajectories leaving the positive quadrant, and red denotes divergent or nonfinite trajectories. Black points represent the displayed attracting set.

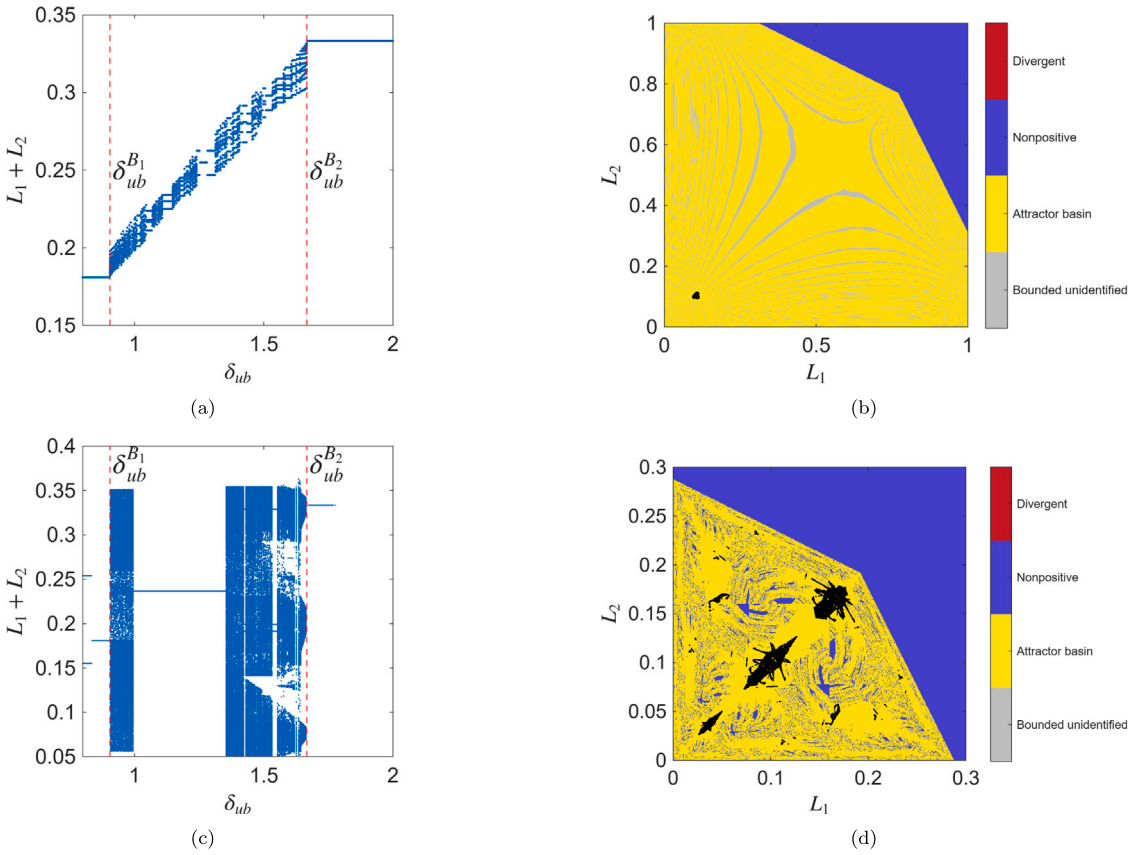


Fig. 11. Economic scenario 6. (a) Bifurcation diagram with respect to δ_{ub}, where $L^* = L_1^* + L_2^*$, when two border-collision bifurcations occur. The simulation uses $\alpha = 7$, $a = 0.165$, $b = 0.07$, $r_A = 0.08$, $K = 0.1$, $\Lambda = 0.13$, $\gamma_{lb} = 0.1$, $\gamma_{ub} = 0.2$, $\delta_{lb} = 0.78$, $L_{1,0} = 0.02$, and $L_{2,0} = 0.01$. (b) Basin diagram for $\delta_{ub} = 1$. (c) Bifurcation diagram with respect to δ_{ub} with $\alpha = 47$ and the remaining parameters unchanged. (d) Basin diagram for $\delta_{ub} = 1.6$ and $\alpha = 47$. In the basin diagrams, yellow denotes the basin of the displayed attracting set, gray denotes bounded but unidentified initial conditions, blue denotes trajectories leaving the positive quadrant, and red denotes divergent or nonfinite trajectories. Black points represent the displayed attracting set.

(b) of Fig. 9, computed for $\gamma_{ub} = 0.125 > \gamma_{ub}^B$, illustrates the post-border-collision regime. In this case, the bounded dynamics is organized around a low-period attractor, showing that the transition beyond the border-collision threshold does not necessarily lead to a chaotic set. Hence, this figure provides a complete numerical illustration of the two destabilization mechanisms predicted analytically for the upper regulatory parameter.

The next two figures illustrate the effect of varying the corridor bounds δ_{lb} and δ_{ub}. In Fig. 10, the analytical results predict two border-collision values for δ_{lb}, namely δ_{lb}^{B2} and δ_{lb}^{B1}, which delimit the interval in which the central fixed point $\mathbb{E}_{93}$ is replaced by the lower-regime fixed point $\mathbb{E}_{13}$. This theoretical structure is clearly reproduced in Fig. 10(a): outside the interval bounded by the two dashed lines, the dynamics is regular, whereas between them more complicated attractors arise. When the adjustment speed is increased, as in Fig. 10(c), the same geometric thresholds still organize the diagram, but the unstable region becomes much wider and chaotic behavior appears, as confirmed by the attractor and basin in Fig. 10(d). Hence, once the borders are fixed, a larger value of α amplifies the destabilizing effect of the switching mechanism.

A similar interpretation applies to Fig. 11, where δ_{ub} is varied. The theoretical thresholds δ_{ub}^{B1} and δ_{ub}^{B2} separate the parameter region in which the upper-regime fixed point $\mathbb{E}_{53}$ may be admissible from the region in which the central fixed point $\mathbb{E}_{93}$ may be admissible. Fig. 11(a) shows that, for a relatively small adjustment speed, the attractor changes exactly when these thresholds are crossed. By contrast, for the larger value of α used in Fig. 11(c), the same thresholds still organize the dynamics, but the observed motion becomes much more irregular and chaotic sets emerge, as shown in Fig. 11(d). This again confirms that the interaction between prudential thresholds and banks' behavioral reactivity is a key determinant of global stability.

6.2. Isoperiodic structure

The one-parameter bifurcation diagrams are complemented by the isoperiodic charts shown in Fig. 12. These panels provide a synthetic view of how the periodicity of the attractor changes in two-parameter planes. In particular, Fig. 12(a) and 12(b) show that

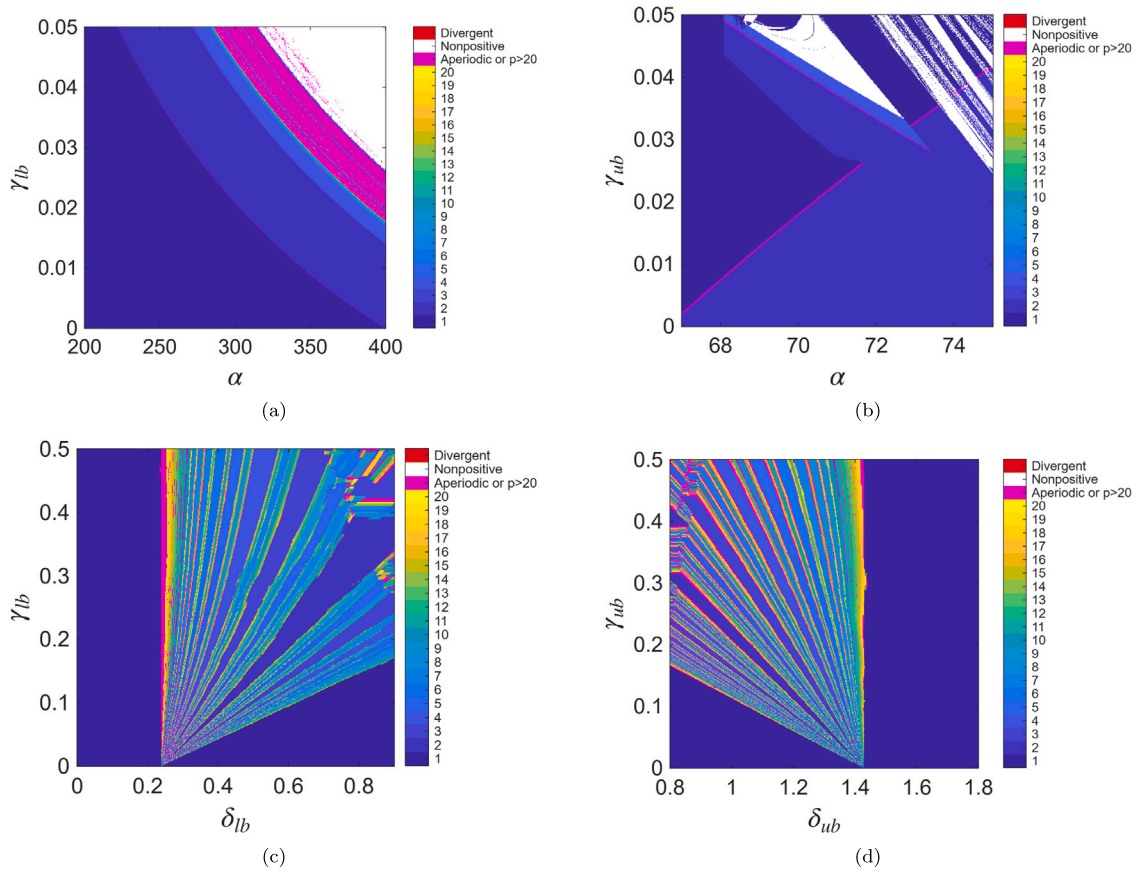


Fig. 12. Two-parameter isoperiodic diagrams. The color bar denotes the detected period of the attracting dynamics, up to period 20. White denotes trajectories leaving the positive quadrant, red denotes divergent or nonfinite trajectories, and magenta denotes aperiodic dynamics or periods larger than 20. Panel (a) shows the (α, γ_{lb}) plane for $a = 0.135$, $\gamma_{ub} = 0.2$, $\delta_{lb} = 0.78$, and $\delta_{ub} = 1$. Panel (b) shows the (α, γ_{ub}) plane for $a = 0.16$, $\gamma_{lb} = 0.1$, $\delta_{lb} = 0.78$, and $\delta_{ub} = 1$. Panel (c) shows the $(\delta_{lb}, \gamma_{lb})$ plane for $\alpha = 15$, $a = 0.135$, $\gamma_{ub} = 0.2$, and $\delta_{ub} = 1$. Panel (d) shows the $(\delta_{ub}, \gamma_{ub})$ plane for $\alpha = 5$, $a = 0.16$, $\gamma_{lb} = 0.1$, and $\delta_{lb} = 0.78$. Other parameters are $b = 0.07$, $r_A = 0.08$, $K = 0.1$, $\Lambda = 0.13$, $L_{1,0} = 0.02$, and $L_{2,0} = 0.01$.

the transition from stability to oscillatory dynamics in the (α, γ_{lb}) and (α, γ_{ub}) planes follows the analytical flip conditions derived in Section 5. Low-period regimes occupy the region close to the stability boundary, while higher-period and chaotic regimes appear as the parameters move away from it.

Fig. 12(c) and 12(d) display the isoperiodic structure in the $(\delta_{lb}, \gamma_{lb})$ and $(\delta_{ub}, \gamma_{ub})$ planes. Their wedge-shaped organization is consistent with the linear relationships between the border-collision thresholds and the corresponding regulatory parameters. In this sense, the numerical results confirm that the LDR-RR parameters do not merely shift the equilibrium level of loans; rather, they reshape the whole geometry of the attractors and their basins.

Overall, the simulations strongly support the analytical results. At the same time, they reveal additional global features, such as coexistence of attractors, sensitivity to initial conditions, and chaotic oscillations, which cannot be inferred from local stability analysis alone. This combination of analytical and numerical evidence provides a coherent description of the lending dynamics generated by the proposed piecewise banking duopoly model.

7. Conclusions

In this paper, we have extended the banking duopoly model with macroprudential policy proposed in [15] to the case in which the banks' CAR remains below the incentive threshold of the Indonesian LDR-RR framework. Unlike the one-sided specification previously studied, the present setting leads to a two-sided regulatory mechanism, because reserve-requirement penalties may become active both when the loan-to-deposit ratio falls below the lower bound and when it exceeds the upper bound.

The analytical investigation shows that the phase space is naturally partitioned into nine regions, each associated with a different smooth subsystem. Within this framework, real and virtual fixed points play distinct roles. Only the diagonal equilibria E_{13}, E_{53}, and E_{93} may become locally asymptotically stable under suitable parameter conditions, whereas boundary equilibria are always unstable and several non-diagonal equilibria remain permanently virtual. Depending on the parameter configuration, the admissible

equilibria may lose stability through flip bifurcations or through border-collision bifurcations. Therefore, the qualitative behavior of the duopoly is determined by the joint action of the adjustment speed α and the macroprudential parameters γ_{lb}, γ_{ub}, δ_{lb}, and δ_{ub}.

The numerical analysis supports these conclusions and clarifies their global implications. The one-parameter bifurcation diagrams reproduce the main theoretical thresholds, while the basin plots and isoperiodic diagrams show that large adjustment speeds or strong regulatory feedback may generate multistability, sensitivity to initial conditions, and chaotic fluctuations in aggregate lending. In this sense, the LDR-RR affects the system not only by modifying the equilibrium loan volumes, but also by reshaping the long-run qualitative dynamics of the banking duopoly.

From an economic viewpoint, the model suggests that the calibration of the macroprudential corridor cannot be separated from the behavioral responsiveness of banks. If the reaction to current profitability is excessively aggressive, or if the reserve-requirement mechanism is too restrictive, the policy may amplify rather than smooth lending fluctuations. Conversely, suitable values of the corridor bounds and of the penalty coefficients may keep the system in a stable regime even when banks operate below the incentive CAR threshold.

In policy terms, the results suggest that, for rural banks with CAR below the incentive threshold, the penalty coefficients should not be calibrated independently of the adjustment speed of bank lending. In particular, when banks react strongly to short-run profitability, an excessively high upper-side penalty γ_{ub} may push the system beyond the flip or border-collision thresholds and generate persistent lending fluctuations. A prudential calibration should therefore keep the relevant penalty coefficient below the corresponding destabilization threshold and should monitor whether changes in the LDR corridor move the system outside the stability region.

Several extensions may be considered in future work. It would be interesting to relax the symmetry assumption between banks, to allow for endogenous or heterogeneous deposit dynamics, and to introduce a time-varying capital ratio instead of a constant κ. Another natural step would be to calibrate the model on disaggregated banking data and to study its interaction with other macroprudential instruments currently used in Indonesia. These extensions could provide a richer description of the joint effects of prudential regulation and competitive behavior on bank lending dynamics.

CRediT authorship contribution statement

Moch. Fandi Ansori: Writing – review & editing, Writing – original draft, Methodology, Investigation, Formal analysis, Conceptualization. **Serena Brianzoni:** Writing – review & editing, Writing – original draft, Methodology, Investigation, Formal analysis, Conceptualization. **Giovanni Campisi:** Writing – review & editing, Writing – original draft, Software, Methodology, Investigation, Conceptualization.

Declaration of competing interest

The authors declare that they have no known competing financial interests or personal relationships that could have appeared to influence the work reported in this paper.

Acknowledgments

Moch. Fandi Ansori gratefully acknowledges Universitas Diponegoro for providing research funding from non-APBN sources through the Riset Kolaborasi Undip (RKU), Indonesia scheme 2026, under grant number 306-196/UN7.D2/PP/V/2026.

Open access funding provided by Università Politecnica delle Marche, Italy within the CRUI-CARE Agreement.

Data availability

The Capital Adequacy Ratio (CAR) data used in Fig. 1 are publicly available from the Indonesian Banking Statistics published by Otoritas Jasa Keuangan (OJK), as cited in the manuscript. The remaining results are based on analytical derivations and numerical simulations, with parameter values reported in the paper. The MATLAB codes used for the numerical simulations are available from the corresponding author upon reasonable request.

References

[1] M.F. Ansori, N. Sumarti, K.A. Sidarto, I. Gunadi, F.H. Gümüş, Mathematical model of bank balance sheet with a macroprudential instrument and its application to banking data, Math. Methods Appl. Sci. 48 (18) (2025) 16789–16803, http://dx.doi.org/10.1002/mma.70127.

[2] M.F. Ansori, Dynamic modeling and optimal control of bank balance sheets under capital adequacy constraints, Int. J. Optim. Control.: Theor. Appl. 16 (1) (2026) 40–53, http://dx.doi.org/10.36922/IJOCTA025250113.

[3] L. Fanti, The dynamics of a banking duopoly with capital regulations, Econ. Model. 37 (2014) 340–349, http://dx.doi.org/10.1016/j.econmod.2013.11.010.

[4] S. Brianzoni, G. Campisi, Dynamical analysis of a banking duopoly model with capital regulation and asymmetric costs, Discret. Contin. Dyn. Syst. - B 26 (2021) 5807–5825, http://dx.doi.org/10.3934/dcdsb.2021116.

[5] S. Brianzoni, G. Campisi, A. Colasante, Nonlinear banking duopoly model with capital regulation: The case of Italy, Chaos Solitons Fractals 160 (2022) 112209, http://dx.doi.org/10.1016/j.chaos.2022.112209.

[6] A. Bacchiocchi, G.I. Bischi, G. Giombini, Non-performing loans, expectations and banking stability: A dynamic model, Chaos Solitons Fractals 157 (2022) 111906, http://dx.doi.org/10.1016/j.chaos.2022.111906.

[7] I. Gunadi, C.A. Harun, Revitalising reserve requirement in banking model: An industrial organisation approach, 2011, SEACEN Occasional Papers.

[8] H. Wonida, S.U. Setiastuti, The effect of monetary, macroprudential policy, and their interaction on bank risk-taking in Indonesia, J. Asian Econ. 96 (2025) 101863, http://dx.doi.org/10.1016/j.asieco.2024.101863.
[9] M.F. Ansori, N. Sumarti, K.A. Sidarto, I. Gunadi, Analyzing a macroprudential instrument during the COVID-19 pandemic using border collision bifurcation, Rect@ Rev. Electrónica Comun. Trab. ASEPUMA 22 (2) (2021) 113–125, http://dx.doi.org/10.24309/recta.2021.22.2.04.
[10] D.M. Satria, C.A. Harun, A.A. Taruna, The macro-prudential aspects of loan-to-deposit-ratio-linked reserve requirement, Appl. Econ. 48 (1) (2016) 24–34, http://dx.doi.org/10.1080/00036846.2015.1073840.
[11] R. Wijayanti, N.M. Adhi P., C.A. Harun, Effectiveness of macroprudential policies and their interaction with monetary policy in Indonesia, in: Measuring the Effectiveness of Macroprudential Policies using Supervisory Bank-Level Data, in: BIS Papers, vol. 110, Bank for International Settlements, 2020, pp. 31–50.
[12] D. Zulverdi, I. Gunadi, B. Pramono, Bank portfolio model and monetary policy in Indonesia, J. Asian Econ. 18 (1) (2007) 158–174.
[13] P.-R. Agénor, L.A.P. da Silva, Macroprudential regulation and the monetary transmission mechanism, J. Financ. Stab. 13 (2014) 44–63.
[14] C. Glocker, P. Towbin, Reserve requirements as a macroprudential instrument: Empirical evidence from Brazil, J. Macroecon. 44 (2015) 158–176, http://dx.doi.org/10.1016/j.jmacro.2015.02.007.
[15] M.F. Ansori, S. Brianzoni, G. Campisi, Bifurcations and complex dynamics in a banking duopoly model with macroprudential policy, Phys. A 641 (2024) 129730, http://dx.doi.org/10.1016/j.physa.2024.129730.
[16] M. di Bernardo, C.J. Budd, A.R. Champneys, P. Kowalczyk, Piecewise-smooth dynamical systems: Theory and applications, Applied Mathematical Sciences, vol. 163, Springer, London, 2008, http://dx.doi.org/10.1007/978-1-84628-708-4.
[17] J. Agung, S.M. Juhro, Y. Kurniati, R. Anglingkusumo, Sahminan, Bank Indonesia policy mix, in: P. Warjiyo, S.M. Juhro (Eds.), Central Bank Policy Mix: Issues, Challenges, and Policy Responses, Springer, Singapore, 2022, pp. 135–151, http://dx.doi.org/10.1007/978-981-16-6827-2_8.
[18] A. Abubakar, Y. Setiawan, Macroprudential policy and institutional arrangement, in: P. Warjiyo, S.M. Juhro (Eds.), Central Bank Policy Mix: Issues, Challenges, and Policy Responses: Handbook of Central Banking Studies, Springer, Singapore, 2022, pp. 93–108, http://dx.doi.org/10.1007/978-981-16-6827-2_6.
[19] P. Warjiyo, Central bank policy mix: Key concepts and Indonesia experience, Bull. Monet. Econ. Bank. 18 (4) (2016) 379–408, http://dx.doi.org/10.21098/BEMP.V18I4.573.
[20] M.A. Dabrowski, D.M. Widiantoro, Effectiveness and conduct of macroprudential policy in Indonesia in 2003–2020: Evidence from the structural VAR models, Eurasian Econ. Rev. 13 (3) (2023) 703–731, http://dx.doi.org/10.1007/s40822-023-00244-w.
[21] Bank Indonesia, Bank Indonesia Regulation No. 12/19/PBI/2010 on minimum reserve requirements for commercial banks in rupiah and foreign currency, 2010, Original title in Indonesian: Peraturan Bank Indonesia Nomor 12/19/PBI/2010 tentang Giro Wajib Minimum Bank Umum pada Bank Indonesia dalam Rupiah dan Valuta Asing.
[22] Otoritas Jasa Keuangan, Indonesian banking statistics, 2024, https://www.ojk.go.id/id/kanal/perbankan/data-dan-statistik/statistik-perbankan-indonesia/Default.aspx. (Accessed 01 April 2025).
[23] Bank Indonesia, Bank Indonesia Regulation No. 8/18/PBI/2006 concerning the Minimum Capital Adequacy Requirement for Rural Banks, 2006, Original title in Indonesian: Peraturan Bank Indonesia Nomor 8/18/PBI/2006 tentang Kewajiban Penyediaan Modal Minimum Bank Perkreditan Rakyat.
[24] L. Gardini, W. Tikjha, Role of the virtual fixed point in the center bifurcations in a family of piecewise linear maps, Int. J. Bifurc. Chaos 29 (14) (2019) 1930041, http://dx.doi.org/10.1142/S0218127419300416.
[25] E.I. Jury, A note on the modified stability table for linear discrete time systems, IEEE Trans. Circuits Syst. 38 (2) (1991) 221–223, http://dx.doi.org/10.1109/31.68301.